1997

Numerical modeling of pulsed eddy current techniques for detection of corrosion and cracks

Kiran Kumar Dasoju
Iowa State University

Numerical modeling of pulsed eddy current techniques for detection of corrosion and cracks

by

Kiran Kumar Dasoju

A thesis submitted to the graduate faculty

in partial fulfillment of the requirements for the degree of

MASTER OF SCIENCE

Major: Computer Engineering

Major Professor: Charles T. Wright

Iowa State University

Ames, Iowa

1997

Graduate College
Iowa State University

This is to certify that the Master's thesis of

Kiran Kumar Dasoju

has met the thesis requirements of Iowa State University

Signatures have been redacted for privacy

Dedicated to my mom and dad

TABLE OF CONTENTS

ACKNOWLEDGEMENTS

I wish to express my most sincere gratitude to my research advisor John. C. Moulder for his guidance and invaluable help for this research. His insight and knowledge has motivated me during my stay at Center for Nondestructive Evaluation. The professional example set by him will always be a source of inspiration. I would like to thank Dr. Norio Nakagawa and Dr James. H. Rose for their valuable help during my research. I wish to thank my committee members Dr. Charles. T. Wright, Dr. Lalita Udpa, Dr. Gurpur. M. Prabhu for their support and encouragement. I am also thankful to Avanindra and Shravan Kumar Dasoju for making my stay in Ames a pleasant experience. I would like to thank all the members of Eddy Current group at Center for Nondestructive Evaluation who made working at the center an enjoyable experience.

I am grateful to my parents, family members and friends for their constant support and encouragement. I wish to dedicate this work to them

1. INTRODUCTION

After many years of service, an aircraft will eventually reach an age where fatigue cracks and corrosion develop in the body of the aircraft. The consequent deterioration in its structure affects the safe operation of the aircraft. Consequently, the ability to determine the degree of corrosion damage and the presence of cracks developed in the airframe is important for both prediction of component performance and its remaining service life. The pulsed eddy current technique has been under development for several years at Iowa State University under the supervision of Mr. John. C. Moulder [1] for detection of corrosion and cracks in multi-layered aircraft structures.

Recently a new swept frequency based layer approximation technique was developed by Satveli, Moulder and Rose [2] for modeling the detection of corrosion in multi-layered aircraft structures. Their approach was based on an absolute comparison of measurement to the solution for the change in impedance of an air-core probe when placed on the defective layered metallic surface. Their approach gave very good agreement of model and experiment, but the practical implementation of the method requires absolute measurements of the coil's impedance over a range of frequencies using an HP4194A impedance analyzer and each measurement took several minutes to complete. Hence there is a need for faster methods. The pulsed eddy current technique can provides this faster approach and is the topic of this thesis.

Initial development of the theory of pulsed eddy current was carried out by Rose et al. [4]. Other authors have also proposed time-domain approaches for detection of corrosion and cracks. Bowler and Harrison [5] have reported on detection of corrosion using pulsed eddy current techniques. Beissner and Fisher [6,7] studied the application of pulsed eddy current

for detection and characterization of small cracks in titanium based jet engine alloys.

In this thesis we study pulsed eddy current based techniques for characterizing both corrosion and cracks in layered metallic structures. Our primary goal is to understand and model the characteristic features of time-domain current-voltage response functions for characterizing corrosion and cracks. This is simpler and faster than frequency domain approaches, and the pulsed eddy current equipment developed for defect detection is less expensive than alternative approaches and easily portable. We take the layer approximation theory [2] for corrosion and the boundary integral method [3] for cracks as the basis for computing the change in impedance of the coil and then compute the transient voltage-current response for step-function excitation of the coil. Considerable effort has been made to reduce the computational complexity of calculations of the change in impedance of the coil. We verified our theoretical results against practical measurements on manufactured simulations of lap joints made from 1 mm thick 2024 aluminum plates, using milled regions to simulate metal lost due to corrosion, and 1 mm thick 2024 aluminum plates with EDM notches to simulate fatigue cracks.

The experimental approach is based on a scanned pulsed eddy current (SPEC) instrument developed in our laboratories by Moulder et al. [1,4]. It measures the transient voltage-current response function for step-function excitation of a coil. This personal-computer based instrument is capable of rapid measurements. Pulsed eddy current systems have important advantages. Since pulsed signals contain a broad range of frequencies, their information content is inherently greater than conventional single or dual frequency signals, they are similar to swept frequency based methods, which sample large number of frequencies, but pulsed eddy current techniques are faster. The step function voltage

excitation gives a spectrum which is inversely proportional to frequency and hence strongly emphasizes the low-frequency components of the signal. Thus pulsed eddy current techniques can provide better discrimination than the frequency domain based methods at low frequencies

The remainder of this thesis consists of three chapters. Chapter Two introduces a general overview of nondestructive testing, then introduces the basic issues in eddy current NDE. Chapter Three explains the theory of the layer approximation with a brief description of the analytical solution for the electric fields in layered conductors. This solution follows closely the description of Dodd and Deeds [8] and the transfer matrix solution of Cheng, Dodd and Deeds [9] for a layered metal. Next we describe Auld's reciprocity formula for computing the change in impedance of a coil due to the presence of a flaw in a layered metal surface, description of layer approximation method is given briefly. Next we describe the computing time problem involved in the computation of change in impedance and propose to use bicubic spline interpolation to reduce the amount of computation. An introduction to interpolation, splines and bicubic splines is also given. Then we propose time-domain based techniques for computing the transient voltage-current response function for step-function excitation of a coil. This chapter also reports the results of calculations modeling pulsed eddy current measurements using a small, right cylindrical, air-core coil placed next to a sample consisting of a single layer of 1 mm thick 2024 aluminum, and also a double layered sample to simulate lap joints. The pulsed eddy current instrument (SPEC) was used to measure the transient response of the coil due to various right-cylindrical flat bottom holes of different radii, and at different distances from the center of the coil and at various positions in between the metal layers. Good agreement was obtained between the calculations and the

measurements. Chapter Four deals with cracks in the metal surfaces. Initially, this chapter gives a brief introduction to the theoretical formulation of the boundary integral based method for computation of change in impedance of a coil placed next to the metal surface containing a tight crack. Then the time domain model for computing the transient response is described. This chapter also reports the results of the time domain based calculations and measurements using right cylindrical coil placed next to a metal sample containing an EDM notch to simulate the crack. The computations and experiments were done for various dimensions of the cracks and also various positions on the metal sample. A good agreement between theory and experiment was found. Finally Chapter Five summarizes the work and draws a number of conclusions.

2. EDDY CURRENT BASED NONDESTRUCTIVE TESTING

2.1 Overview of Nondestructive Evaluation

Defects of different nature and dimensions may be introduced into materials or components either during manufacture or in service that will influence their subsequent performance and useful service life . It is therefore necessary to have a reliable method to detect the defects introduced at the manufacturing stage and also during use. Nondestructive testing is used for prediction of component performance and remaining service life, based on its ability to detect flaws, measure dimensions and assess material characteristics.

The basic approach of nondestructive testing is to detect changes in the relevant signal obtained from the probing energy / test surface interaction. Changes in the signal are associated with the presence or absence of flaws or undesirable material properties. The selection of the nondestructive testing method is dependent on the physical properties of the testpeice and the flaw.

The two primary uses of nondestructive testing are testing of newly manufactured components to make sure they comply with the design specifications and periodic testing of the component to determine whether the part is suitable for continued usage. Nondestructive testing is most commonly used in places where component failure causes huge losses such as in airplanes, offshore drilling platforms, petrochemical plants, gas transmission lines and ground transportation systems and structures

Using well established physical principles, a number of nondestructive testing techniques have been developed [10] which will provide information on the quality of a material or component without altering the properties or damaging the test material. The most

common techniques in use are radiography, ultrasonic testing,, electrical methods, magnetic methods, liquid penetrant method. All these nondestructive testing methods co-exist and, depending upon the application, can be used singly or along with other techniques. There are some common features among these test methods but they are complimentary to one another. The fact that, for example, ultrasonic testing can reveal both internal and surface flaws does not necessarily mean that it will be the best method for all inspection applications. Much will depend on the type of flaw present and the shape and size of the components to be examined.

• Radiographic inspection techniques use penetrating radiation to visualize the internal structures of components, materials, and assemblies. The approach requires a source of electromagnetic radiation that can penetrate the item being examined during exposure. As the radiation passes through the test object, it will be reduced in intensity depending on the type of radiation source and test material. The radiation that succeeds in reaching the far side of the item is detected using X-ray sensitive film, cameras, or other image sensing devices. This technique is used for detecting internal defects, surface defects and the correctness of part assemblies, it can be used for many materials but there are restrictions on the maximum thickness of the test sample .

• Ultrasonic testing is based on the fact that mechanical waves travel well through many materials, especially metals, and can be used to determine the structure-critical material irregularities. Sound waves travel at a rate which is defined by the material's physical properties like elasticity, density and homogeneity. The observation of the change in the propagation characteristics can determine the change in a test sample's physical

properties. This technique is most commonly used for determination of metal thickness, internal flaws and also surface flaws.

• Electrical methods induce eddy currents in the test sample and from the assessment of the various effects, deductions can be made about the nature and condition of the test sample. The details of this method are discussed later in this chapter. This method can be used for any metal for detection of surface defects, subsurface defects and to measure the thickness of non-conductive coating such as paint on a metal.

• Magnetic particle method is based on the fact that ferromagnetic materials develop strong internal magnetic fields when an electric current is passed through the part. When the internal magnetic field encounters any change in magnetic permeability due to factors like open fissures or localized defects, the magnetic field is often forced outside of the material surface. This leakage field will attract any other ferromagnetic materials that may be close to the leakage site. Particles with an affinity for leakage fields are passed over each part by sprinkling them or by flowing over the surface of a test sample. These particles are attracted to the leakage field due to the defects and assume the patterns which define the shapes and contours of the field-disturbing discontinuity.

• Liquid penetrant method is used for the detection of defects which break the surface; it can be used for any metal, many plastics, glass and glazed ceramics. The principle of the technique is that a liquid is drawn by capillary attraction into the defect and, after subsequent development, any surface-breaking defects may be rendered visible to the human eye by using UV radiation to excite the fluorescent dye.

2.2 Principles of Eddy Current Testing

2.2.1 Basic Principles

Eddy current NDE makes use of eddy currents for flaw characterization. It is typically carried out through an eddy current probe driven by a time harmonic current source. A schematic diagram is shown in Figure 2.1. The eddy current probe is a coil carrying alternating current and when it is placed near a conductive material, the current passing through the coil generates a magnetic field in an electrical conductor in its vicinity, as shown

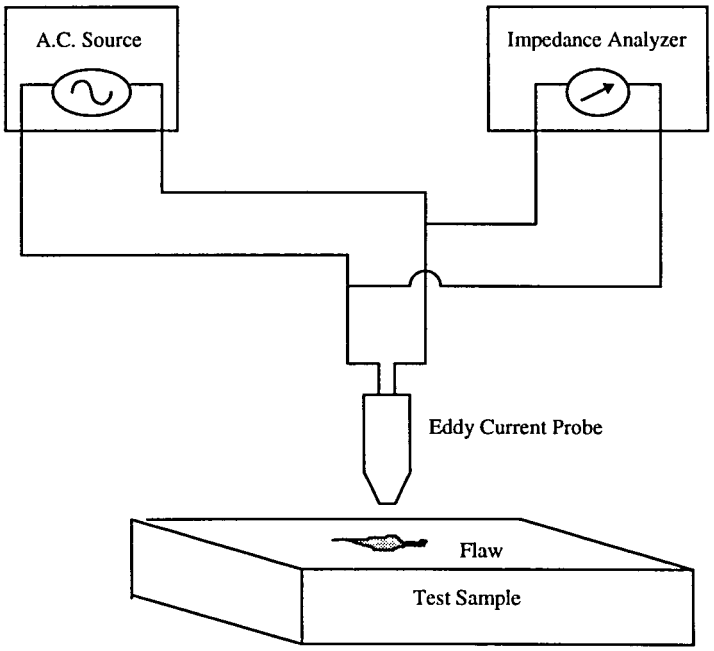

Figure 2.1: Schematic diagram of an eddy current setup for NDE.

in Figure 2.2. The associated magnetic field $\boldsymbol{H}$ induces the flow of secondary currents, i.e. eddy currents, which follow circular paths in planes perpendicular to the direction of $\boldsymbol{H}$, which is defined by Eq. (2.1)

$$\text{curl } \boldsymbol{H} = \boldsymbol{J}. \qquad (2.1)$$

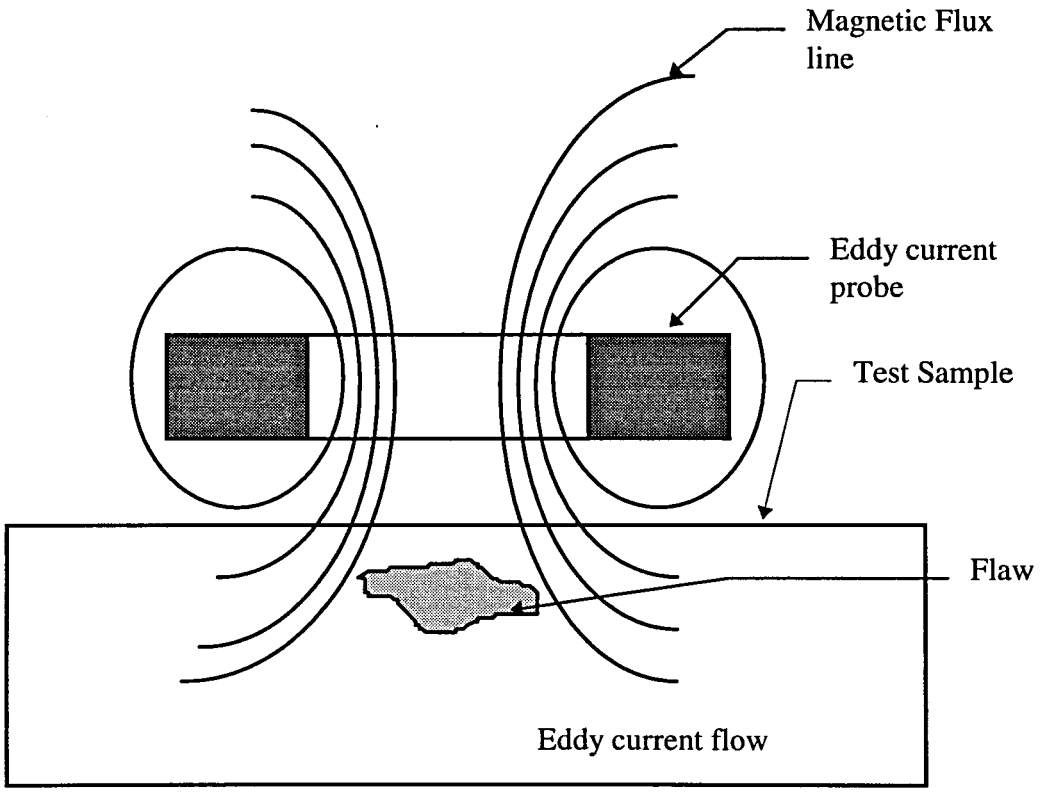

Figure 2.2: Magnetic field coupling of eddy current probe coil and metals under test

The induced eddy current in the conductor will produce a secondary magnetic field which is in opposition to the primary magnetic field; this secondary magnetic field will interact with the primary magnetic field and reduce the amount of flux, resulting in change in impedance of the coil. If the material contains a discontinuity on or below the surface of the test sample, then there is a change in the distribution and magnitude of eddy currents flowing in the vicinity of the discontinuity as shown in Figure 2.3B. This change in flow results in change in magnetic field produced by the eddy currents which results in a change in the impedance of the coil.

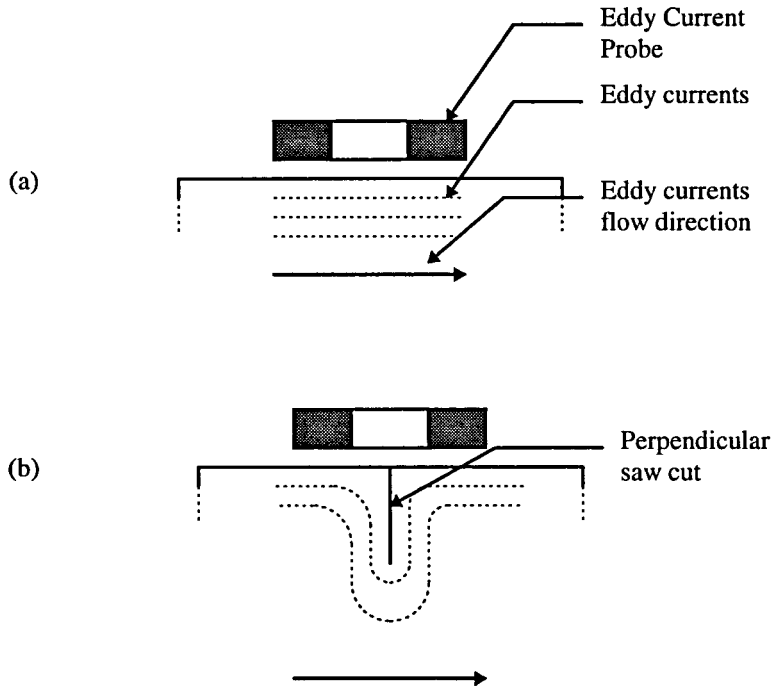

Figure 2.3: Schematic diagram showing flow of eddy currents (A) test sample with out flaw (B) test sample with perpendicular saw cut flaw

2.2.2 Factors Affecting Eddy Current Flow

Eddy currents flow in closed loops in the test sample over which the probe is placed. The magnitude and phase of the eddy currents will depend on various factors like electrical and magnetic properties of the material, presence of defects or discontinuities in the test sample and the magnitude of the magnetic field produced by the coil.

A magnetic field $\boldsymbol{H}$, will produce a magnetic flux density, $\boldsymbol{B}$ whose relation in vacuum is given by Eq. (2.2)

$$\frac{B}{H} = \mu_0 . \qquad (2.2)$$

where μ_0 is magnetic permeability of vacuum whose value is $4\pi \times 10^{-7}$ henry per meter. The magnetic flux density induced in a material for a given magnetizing field is given by Eq. (2.3)

$$\frac{B}{H} = \mu_0 \mu_r \tag{2.3}$$

where μ_r is relative magnetic permeability.

Relative permeability is not constant for any particular ferromagnetic material but varies with the magnitude of the magnetizing force. The strength of any induced eddy currents will also vary considerably and will increase with an increase in relative permeability, hence techniques used for non-magnetic and ferromagnetic materials may differ. Small variations in permeability may have a greater effect on eddy currents than small changes in electrical conductivity. This is particularly true at low frequencies.

When a coil is energized in air the recording instrument gives some signal value, even in the absence of a test sample. When the probe is brought nearer to the sample the signal changes and the magnitude of change increases until the coil is directly on the conductor. The magnitude of eddy currents induced in the test sample due to the magnetic field of the coil decreases as the coil moves away from the test sample. Changes in spacing between the coil and the test sample surface are termed lift-off. The lift-off effect is important due to the fact that a minute change in lift-off may cause considerable decrease in magnitude of eddy currents induced in the test sample.

At the component edges the flow of eddy currents is distorted as the eddy currents are unable to flow beyond this limiting barrier; this is called edge-effect. The magnitude of edge effect is very large, hence inspection at edges is not reliable.

The eddy currents in the test sample are not distributed uniformly throughout; they are densest on the surface of the sample, just beneath the coil and they gradually become less dense with increasing distance from the surface of the sample. At some distance beneath the surface of the test sample the eddy currents become negligible; this phenomenon is called the skin effect. The eddy current density decreases exponentially with distance into the test sample; the distance at which the magnitude of eddy current is decreased by $1/e$ (~37%) of its value at the surface is called the skin depth. This decay is defined by Eq. (2.4)

$$\delta = \frac{1}{\sqrt{\pi f \mu \sigma}} \tag{2.4}$$

where δ is skin depth, σ is conductivity of the test sample, μ is permeability, f is the frequency of operation of the coil.

Skin depth is not constant for any particular material but it decreases as the test frequency increases. Thus the depth of penetration for a given material is controlled by the frequency. The value of δ, in relation to the specimen thickness, is a useful method of determining the inspection frequency to be used in eddy current applications. Typically the inspection frequencies used in electrical techniques range from 20 Hz to 10 MHz. The actual frequency to be used is usually determined by trying to attain optimum sensitivity at the desired penetration depth. For non-magnetic materials, the choice of inspection frequency becomes relatively simple when detecting surface flaws only, frequencies as high as possible (several MHz) are used, but for detection of subsurface flaws at a considerable depth the inspection frequency should be low, sacrificing sensitivity. Ferromagnetic materials demand very low frequencies because of relatively low penetration depth in these materials. Higher frequencies can be used to inspect surface conditions only.

In general there are several different coil arrangements which can be used in eddy current testing. A single primary solenoid type coil may be used for the routine inspection of cylindrical bars or tubes. The test piece is passed through the coil. Variations of the coil impedance as the testpiece moves indicates the presence of the flaws.. For enhanced sensitivity, transformer probes, which have separate transmitting and receiving coil windings, may be used if, for example, deep penetration of eddy currents is required in the material under test. For many tests and inspection purposes, a coil or coils are mounted in a holder as an inspection probe as shown in Figure 2.4. The coil is usually wound on an air core or ferrite core and the coil is protected by a plastic casing. The single coil probe shown in Figure 2.4 is ideal for the detection of surface defects such as small cracks. The probe should be held normal to the component surface, otherwise incorrect indications could occur. The probe may be held in a jig to ensure that it is always normal to the testpiece surface.

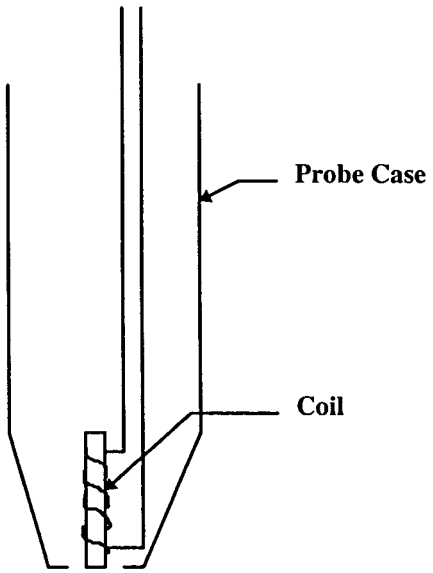

Figure 2.4: Surface probe for defect detection

2.3 Forward Problem and Inverse Problem

Modelling of flaw detection may be conveniently divided into two problems : the forward problem and the inverse problem. These are discussed in this section

2.3.1 Forward Problem

The forword problem deals with determination of fields and changes in coil impedance from the given physical characteristics of the test sample, flaw, and the geometry and characteristics of the coil. In this thesis we use an analytical solution for the impedance of an air-core coil over a layered metal derived by Cheng [11] and by Dodd and Deeds [8] for determining the coil impedance for the flawless case, and for determining the change in impedance of the coil in the presence of the flaw we use a perturbation theory-based solution derived by Rose et al. [2,3,12]. Various solutions have been proposed for different cases of the forward problem such as an analytical solution for the impedance of an air core coil over a multilayered metal by Cheng, Dodd and Deeds [9]. Auld [14,15] developed an exact reciprocity-based formula to predict the change in impedance of the coil. The disadvantage of the Auld's formula is that it requires determination of the exact electric field in the region of the flaw. Nakagawa et al. [16,17] have developed a BEM based model which is capable of simulating of eddy currents in generic inspection geometry.

2.3.2 Inverse Problem

The inverse problem is to characterize the defect, given the change of impedance of the probe at one or more frequencies. This problem is more indirect. A possible solution would be to solve the forward problem for various defect dimensions and tabulate the results. Next compare the change in impedance obtained through actual measurement of the defective sample with the tabulated results. A match might indicate the dimensions of the defect. For

example, Sethuraman and Rose [26] used this approach to determine the thickness and conductivity of metal coatings from swept-frequency eddy current signals. A comparison was made between measurement and a look-up table based on analytical solution for the impedance of an air-core coil over a layered metal derived by Cheng [11] and by Dodd and Deeds [8].

2.4 Eddy Current Inspection Techniques

Swept-frequency eddy current and pulsed eddy current methods are the two methods mainly used at CNDE for eddy current inspection. Since the diffusion of eddy currents into metals is governed by the skin effect, the main idea of the swept-frequency eddy current approach is to use a number of different frequencies to excite the coil. As mentioned earlier, the skin depth changes with frequency, conductivity and permeability of the materials under inspection. Hence, use of different excitation frequencies gives more depth information; lower frequencies have larger skin depth and they penetrate more deeply into the metals. Higher frequencies have smaller skin depth; they can be used to detect surface flaws. Since eddy currents interact with ferromagnetic materials in a way that depends on the frequency, using this technique to characterize magnetic metals is a promising application as well.

The pulsed eddy current method (PEC) is a time domain method wherein the coil is excited by step-function voltage. It gives essentially the same information as the swept frequency method because the frequency domain equivalent of a step function covers a broad spectrum. It contains low frequencies as well as high frequencies as shown in Figure 2.5. The advantage of the PEC method over the swept-frequency method is that the PEC measurement is very fast (~1-10 ms) whereas in the swept frequency method there is a need to take measurements at 100 or more frequencies in the desired band. Comparatively the pulsed eddy

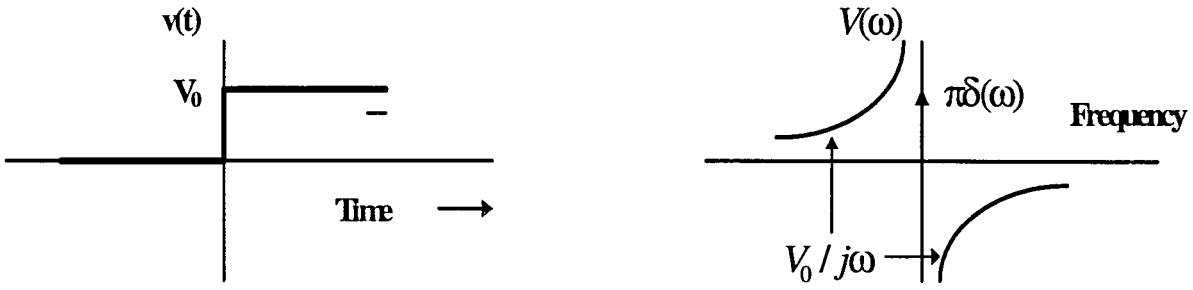

Figure 2.5: Step function voltage and its frequency domain spectrum

current method can be thousands of times quicker than the swept-frequency eddy current method.

2.5 Applications of Eddy Current Techniques

Eddy current test techniques are used for routine inspection of aircraft undercarriage wheels. The wheel is placed on a turntable and the probe coil, which is mounted at the end of an adjustable arm, is positioned near the bottom of the wheel. As the wheel turns on the turntable the probe moves up slowly along the wheel, thereby making a helical search pattern. Eddy currents are used to detect not only cracks, but also corrosion of hidden surfaces, for example, within aircraft structures. It is a comparative technique where the readings made in an area of suspected corrosion are compared with readings taken on a corrosion free surface. Eddy current based techniques can be used for the identification and sorting of materials. The ability of eddy current techniques to determine the conductivity of a material has been utilized for the purpose of checking areas of heat-damaged skin on aircraft structures. The eddy current testing techniques can also be used for measuring the thickness of either conducting or non-conducting coatings on ferrous or non-ferrous base materials.

3. PULSED EDDDY CURRENT TECHNIQUE FOR DETECTION OF CORROSION

Satveli, Moulder, Wang and Rose [2] have recently developed a new perturbation method for computing the change in impedance induced by a three-dimensional defect in layered metallic structures. The layer approximation assumes that the defect is not crack like, that it localized, and that either the relative change in conductivity introduced by the defect is very small or that the sample is nearly one dimensional in the region where coil's electric field is significant. The layer approximation has been tested for a benchmark problem and in this case the agreement between the layer approximation, measurement and more exact theory was excellent. But the measurements required using an HP 4194A impedance analyzer and as the frequency was varied from 2.5 to 50 kHz, it took several minutes to complete the swept frequency measurement. The code written to calculate the electric field, and hence the change in the impedance, took three hours for execution.

In this chapter we describe faster approaches adopted in both theoretical calculations and experimental measurements, while retaining the positive features of the frequency domain approach of Satveli *et al.* The pulsed eddy current method is the faster approach used for experiment. Since pulsed signals contain a broad range of frequencies, their information content is inherently greater than conventional single or dual-frequency signals. In this way, they are akin to swept-frequency measurement methods [18], which sample a large number of frequencies. Our approach is based on a pulsed eddy current instrument developed in our laboratories. It measures the transient current-voltage response function for step-function excitation of a coil. The PC-based instrument is capable of rapid, linear quantitative measurements. The majority of time consumed for theoretical calculations was due to the

requirement to calculate the electric field at many points in the region of significant electric field, so interpolation was used to reduce the number of calculations necessary. A two-dimensional interpolation scheme was used.

3.1 Theory

This section explains the forward calculation adopted for this study. We compute the change in current induced in a small right cylindrical air-core coil placed to next to a layered metal structure with N-layers with a localized defect when compared to the current when the coil is placed over a defect-free sample. The calculation proceeds by first finding the change in coil impedance, ΔZ, by using a layer approximation [2]. This was done in two steps, first using Auld's exact reciprocity-based formula the change in the eddy-current signal is found. This formula predicts the change in impedance if the exact electric field in the region of the defect is known. Second, Cheng, Dodd and Deed's formulas are used to approximate the electric field over the support of the defect. By combining the two steps above, the signal, ΔZ, is found.

3.1.1 Layer Approximation

The concept of the layer approximation described in this chapter determines the change in impedance of an air-core probe due to the presence of a flaw in a layered metal structure by employing a perturbation approach. Perturbation methods are often used to provide solutions to physical problems whose solutions are otherwise too difficult or time consuming. The geometry of the sample and the probe are shown schematically in Figure 3.1. Figure 3.1 shows the probe placed on a layered sample with lift off of l_1 and the

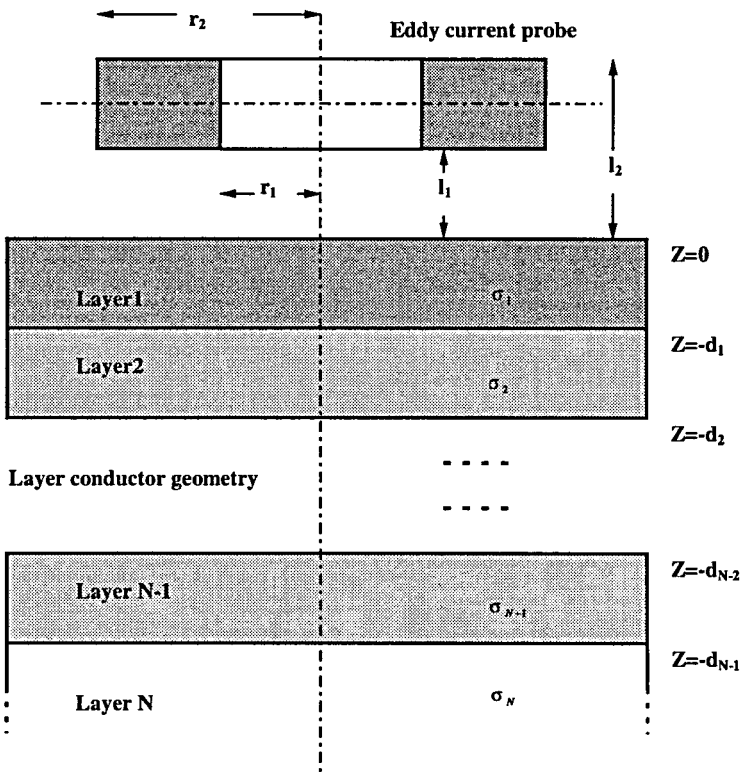

Figure 3.1: Geometry and dimensions of sample and probe

sample consists of N metal layers with conductivity denoted by σ_1 to σ_N. The interfaces between the metal layers are located at depths z= -d_1 to z= -d_N beneath the vacuum-metal interface at z=0. The change in impedance of the probe is calculated by using Auld's reciprocity-based formula. We imagine measuring the frequency-dependent impedance, Z_f, of a small right cylindrical air-core coil placed next to a layered metal structure with N layers and a localized defect as shown in Figure 3.2B. Next we imagine measuring the impedance, Z_0 , of a defect free reference sample as shown in Figure 3.2A. Auld's reciprocity formula given by Eq. (3.1), determines the change in impedance when the eddy-current probe is placed next to a non-magnetic metal:

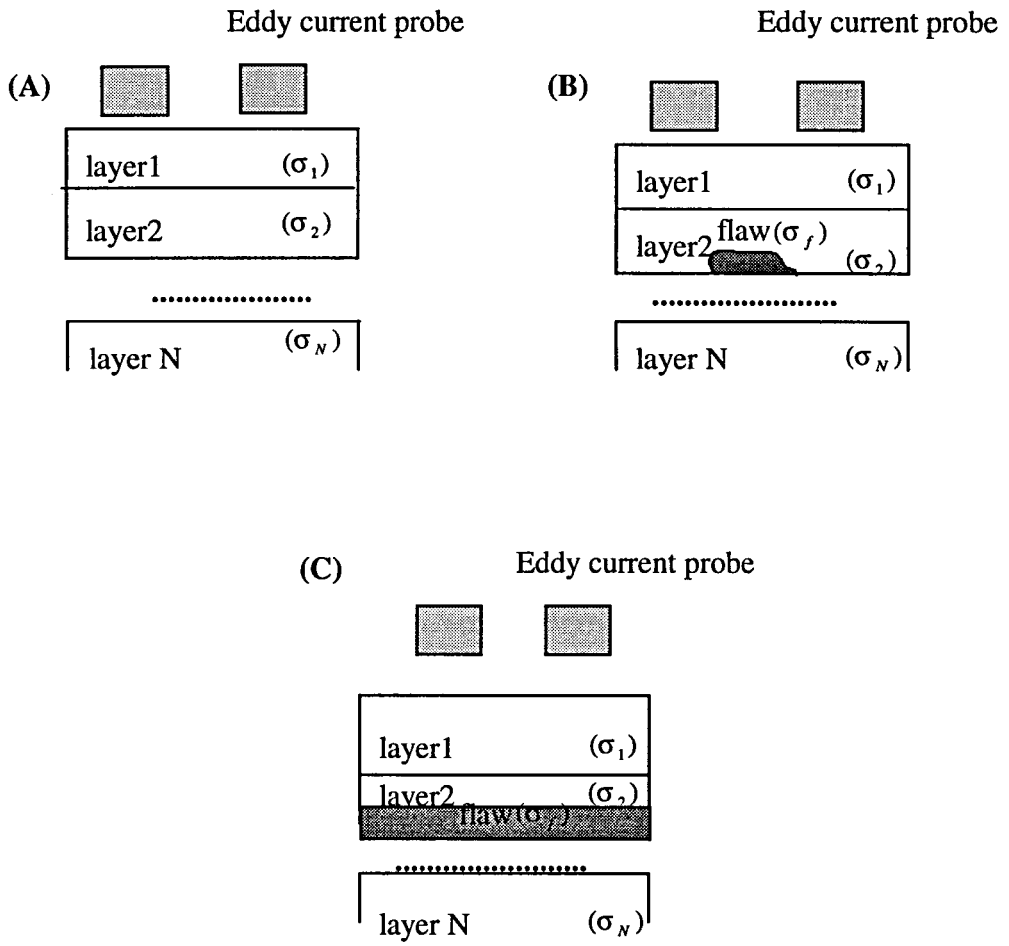

Figure 3.2: (A) Shows the defect-free reference sample. (B) Shows the layered sample with defect (shaded area). (C) Shows the additional hypothetical layer whose conductivity is the same as that of the flaw.

$$\Delta Z(\omega) = -\frac{1}{I^2}\int d^3 y \Delta\sigma(y) E_0(\omega, y) \cdot E_f(\omega, y) \qquad (3.1)$$

$$\Delta\sigma = \sigma - \sigma_0 \qquad (3.2)$$

denotes the difference in conductivity between the concuctivity of the flaw and the concuctivity of the reference sample, and

I is the current in the coil,

ω is the angular frequency,

y is the spatial coordinate,

E_f is the electric field in the flawed part,

E_0 is the electric field in the reference part.

Eq. (3.1) is particularly useful for perturbation theory because it only requires that E_0 and E_f be estimated in the region of the defect, since $\delta\sigma$ is zero elsewhere. It is not necessary to estimate electric fields in the region of the coil.

The next step is to calculate the electric fields; this is done using the vector potential, $\bar{A}$, and the Coulomb gauge $\nabla \cdot \bar{A} = 0$. The relation between vector potential and the electric field is given by Eq. (3.3)

$$\bar{E} = -\frac{\partial \bar{A}}{\partial t} \tag{3.3}$$

The vector potential $\bar{A}$, in a non-magnetic, isotropic, linear and homogeneous medium is governed by the following partial differential equation

$$\nabla^2 \bar{A} = \mu_0 \bar{j}_{ext} + \mu_0 \sigma \frac{\partial \bar{A}}{\partial t} + \mu_0 \varepsilon \frac{\partial^2 \bar{A}}{\partial t^2} \tag{3.4}$$

where μ_0 denotes the permeability of free space, while ε denotes permittivity. Considering that external current is sinusoidal and that the coil is cylindrical, substituting the equation of external current and vector potential in cylindrical coordinates in Eq. (3.4) and ignoring the displacement current, the final form for the partial differential equation for the vector potential is given as

$$\frac{\partial^2 A}{\partial r^2}+\frac{1}{r}\frac{\partial A}{\partial r}-\frac{1}{r^2}A+\frac{\partial^2 A}{\partial z^2}=\mu_0 j_{ext}+\mu_0\sigma j\omega A\,. \tag{3.5}$$

Solving Eq. (3.5) for each layer, the general solution for every layer is given by

$$A(r,z)=\int_0^\infty\left(C(\alpha)e^{z\sqrt{\alpha^2+j\omega\mu\sigma}}+B(\alpha)e^{-z\sqrt{\alpha^2+j\omega\mu\sigma}}\right)\left(J_1(\alpha r)+D(\alpha)Y_1(\alpha r)\right)d\alpha\,. \tag{3.6}$$

Here J_1 and Y_1 are integer Bessel functions of order 1 of the first and second kind. The coefficients B and C are different for each layer. These coefficients are obtained from a transfer matrix solution based on Cheng, Dodd and Deeds [9]

The interface conditions combined with Eq. (3.6) and the boundary conditions yield a set of 2N+2 linear equations in terms of 2N+2 unknowns for each α. These simultaneous linear equations can be represented by a recursive relation given by Eq. (3.7), from which the coefficients B and C for each layer can be determined

$$\begin{pmatrix}C_{n-1}\\B_{n-1}\end{pmatrix}=\begin{pmatrix}\frac{\alpha_n+\alpha_{n-1}}{2\alpha_{n-1}}e^{-d_{n-1}(\alpha_n-\alpha_{n-1})} & \frac{\alpha_{n-1}-\alpha_n}{2\alpha_{n-1}}e^{d_{n-1}(\alpha_n-\alpha_{n-1})}\\ \frac{\alpha_{n-1}-\alpha_n}{2\alpha_{n-1}}e^{-d_{n-1}(\alpha_n-\alpha_{n-1})} & \frac{\alpha_n+\alpha_{n-1}}{2\alpha_{n-1}}e^{d_{n-1}(\alpha_n-\alpha_{n-1})}\end{pmatrix}\begin{pmatrix}C_n\\B_n\end{pmatrix}, \tag{3.7}$$

where n=1.....N and $\alpha_n=\sqrt{\alpha^2+j\omega\mu_0\sigma_n}$. The coefficients are determined by substituting n=0 and solving for C's and B's. Once C_0 is known , the coefficients for n=1,..,N can be determined recursively from Eq. (3.7) and the boundary condition B_N=0.

Using the relation $E=-j\omega A$, the electric field in the nth layer is given by

$$E_n(r,z,r_0,h)=-j\omega\int_0^\infty d\alpha[C_n(\alpha,r_0,h)e^{\alpha_n z}+B_n(\alpha,r_0,h)e^{-\alpha_n z}]J_1(\alpha r)\hat{e}_\theta \tag{3.8}$$

for a delta function current filament of radius r_0 at a height h above the metal surface.

Hence to find the change in impedance of the probe, initially the electric field is calculated for the sample without flaw and with flaw using a combination of formulas given by Dodd and Deeds [8] and the transfer matrix solution of Cheng, Dodd and Deeds [9]. Then Auld's formula is used to compute the change in impedance using the electric field so computed. The main disadvantage of Auld's formula is that it requires the determination of the exact electric field in the region of the flaw. The electric field in the presence of flaw depends on the shape and size of the flaw and does not have an exact analytical solution, hence there is need for approximations. Approximate solutions for ΔZ can be obtained by substituting in guesses for $\overline{E}_f$. These guesses are computed using perturbation theory. The approximation adopted to solve the above stated problem is called the layer approximation. The layer approximation assumes that in the presence of the localized defect either the change in conductivity is sufficiently small or that the defect itself can be nearly approximated by a layer (over the region influenced by the electric field of the coil). An additional hypothetical layered sample is imagined, this sample is imagined to be same as original sample except that it contains an extra layer that has the conductivity of the defect. Figure 3.2 shows the schematic representation of the assumption for the case of a flat bottom hole-like defect between the layers.The additional layer is chosen to overlap the support of the defect but otherwise to be as thin as possible. The electric field E_f is computed for this hypothetical sample and it is replaced for **E** in the reciprocity formula for change in impedance mentioned earlier.

As shown by Eq. (3.8), we see that the electric field is a function of angular frequency ω and spatial coordinate y. Hence for finding the change in impedance we have to first find

the electric field at every point in the region of interest in the layered metal sample. The electric field is calculated at positions along length and along the depth of the flaw under consideration resulting in calculation of electric field at the points on the virtual grid on the area of interest which is defined as a rectangle as shown in Figure 3.3. From observation it has been seen that for finding the change in impedance to a reasonable accuracy the electric field has to be calculated at sufficiently large number of points along length and depth of the region of interest, and the time taken in computation of the change in impedance using electric field values at these large number of points is large, so in order to reduce the computation time we used the method of interpolation. In the following section a detailed description of interpolation is given with a description of the type of interpolation used for two-dimensional interpolation.

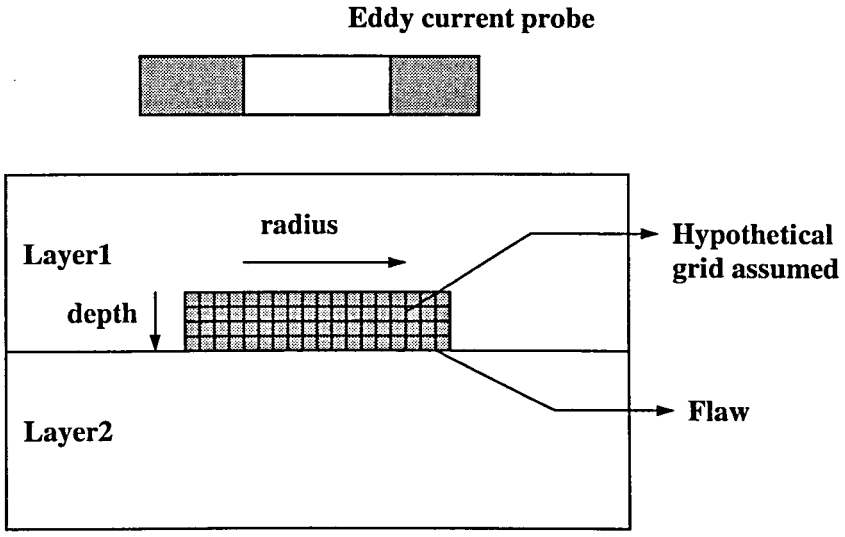

Figure 3.3: Schematic diagram showing the hypothetical grid chosen for computation.

3.2 Interpolation

In the case described earlier where we know the value of the function $E(\omega, y)$ at a set of points in space in the metal in the region of the flaw , even though we have the analytical expression for **E**, due to the computational constraint we cannot compute a sufficient number of points to give a reasonably smooth curve. The task is now to estimate E for arbitrary y by, in some sense, drawing a smooth curve through the y_i. If the desired y lies between the largest and smallest of the y_i's, the problem is called interpolation. Interpolation schemes must model the function between known points by using some plausible functional form. The form should be sufficiently general to approximate large classes of functions might arise in practice.

Conceptually, the interpolation [19] process has two stages: (1) Fit an interpolating function to the data points provided. (2) Evaluate that interpolating function at the target point y. But this two-stage method is inefficient in practice; it is computationally less efficient and more susceptible to round off error than methods which construct a functional estimate f(x) directly from the N tabulated values every time one is desired. Most practical schemes start at a nearby point $f(x_i)$, then add a sequence of decreasing corrections, as information from other $f(x_i)$'s is incorporated. The procedure typically takes $O(N^2)$ operations. If all the points chosen are relatively error free then the last point that is chosen will have the smallest correction, hence this error can be used as bound on the error. Local interpolation using a finite number of nearest neighboring points gives interpolated values f(x) that do not, in general, have continuous first or higher derivatives. That happens because as x crosses the tabulated values x_i, the interpolation schemes switches which tabulated points are the local ones, but in the case of stiff systems, like the one considered here where

the function varies at a nonuniform rate, one must use stiffer interpolation, as provided by the spline function. A spline is a polynomial between each pair of tabulated points, but one whose coefficients are determined "slightly" nonlocally. The nonlocality is designed to guarantee global smoothness in the interpolated function up to some order of derivative. Usually cubic splines are used because they provide continuity up to the second derivative. The number of points used in an interpolation scheme is called the order of the interpolation. Increasing the order does not necessarily increases accuracy; for example, if the added points are distant from the point of interest x, the resulting higher order polynomial, with its additional constrained points, tends to oscillate wildly between the tabulated values. This oscillation may have no relation at all to the behavior of the true function.

3.2.1 Cubic Spline Interpolation

In this section, we review the definition of the cubic spline. which is used in this thesis for interpolation, and its derivation so that the reader can have a better understanding of the reason it was chosen for interpolation.

Through any two points there is a unique line. Through any three points a unique quadratic, etc. Then the interpolating polynomial through these points is given by Lagrange's classical formula, given below by Eq. (3.9).

$$P(x)=\frac{(x-x_2)(x-x_3).....(x-x_N)}{(x_1-x_2)(x_1-x_3).....(x_1-x_N)}y_1+...+\frac{(x-x_1)(x-x_2).....(x-x_{N-1})}{(x_N-x_1)(x_N-x_2)....(x_N-x_{N-1})}y_N \qquad (3.9)$$

where the polynomial P(x) is of degree N-1 through N points $y_1=f(x_1)$, $y_2=f(x_2)$,.....$y_N=f(x_N)$.

Considering that we have a tabulated function of N points, considering only one particular interval between x_j and x_{j+1}. Using the lagrange's formula given by Eq. (3.9) the interpolation formula between these two points is given by Eq. (3.10) and Eq. (3.11).

$$y = Py_j + Qy_{j+1}, \tag{3.10}$$

where

$$P = \frac{x_{j+1} - x}{x_{j+1} - x_j}, \qquad Q = 1 - P = \frac{x = x_j}{x_{j+1} - x_j}. \tag{3.11}$$

Let us assume that we have another set of values given by function y″, and let us assume for the moment that y″ does not indicate the second derivative of function y. If the values of y″ ,*i.e.* y''_j and y''_{j+1}, are used as linear coefficients of two linearly independent cubic polynomial terms (which do not spoil the agreement with the tabulated functional values y_j and y_{j+1} at the end points x_j and x_{j+1}), then any choice of y''_j and y''_{j+1} using these values the Eq. (3.10) can be rewritten as

$$y = Py_j + Qy_{j+1} + Ry''_j + Sy''_{j+1}, \tag{3.12}$$

where R and S are defined by

$$R = \frac{1}{6}(P^3 - P)(x_{j+1} - x_j)^2, \qquad S = \frac{1}{6}(Q^3 - Q)(x_{j+1} - x_j)^2. \tag{3.13}$$

Considering Eq. (3.11), Eq. (3.12), and Eq. (3.13), we see that P and Q depend on the intervals chosen and the independent variable x. R and S are dependent on P, Q and the intervals chosen. The interpolating polynomial depends on the given values of the function to be interpolated, hence if one is given the independent variable, the value of its function can be computed easily.

Taking the derivative of Eq. (3.12) and using the definitions of P, Q, R and S the first derivative of y is

$$\frac{dy}{dx} = \frac{y_{j+1} - y_j}{x_{j+1} - x_j} - \frac{3A^2 - 1}{6}(x_{j+1} - x_j)y''_j + \frac{3B^2 - 1}{6}(x_{j+1} - x_j)y''_{j+1} \tag{3.14}$$

and the second derivative is given by

$$\frac{d^2y}{dx^2} = Ay_j'' + By_{j+1}''. \tag{3.15}$$

Eq. (3.15) shows that the y'''s chosen are second derivatives of y.

The cubic spline is analogous to mechanical splines, which are flexible strips of an elastic material, usually wood or plastic. The mechanical spline is secured by means of weights at the points of interpolation called knots. The spline assumes that shape which minimizes its potential energy, and beam theory states that this energy is proportional to the integral with respect to arc length of the square of the curvature of the spline.

If the mathematical spline is a function represented by s(x) and if the slopes are small, the second derivative $s''(x)$ approximates the curvature, and the interpolating spline s(x) is computed such that the integral described above is minimized.

Assuming that the mechanical spline does not break, we would expect s and s' to be continuous. Elementary beam theory further suggests that s(x) is a cubic polynomial between each adjacent pair of knots, and adjacent polynomials join continuously where first and second derivatives continuous.

until now we have assumed that we are taking some random values for y'', but in this case but then the value of the first derivative computed from Eq. (3.14) would not be continuous across the boundary between two intervals. The key idea of the cubic spline is to require this continuity and to use it to obtain equations for the y_i''. The equations for the y_i'''s can be obtained by forcing the continuity on first derivative by setting its value to $x=x_j$ in the interval (x_{j-1}, x_j), equal to the same equation evaluated for $x=x_j$ but in interval (x_j, x_{j+1}).

This gives N-2 linear equations in N unknowns, y_i'' , i=1,...N. Therefore there is a two parameter family of possible solutions. So for a unique solution using the boundary conditions at x_1 and x_N , the N unknowns are reduced to N-2 unknowns.

The above described cubic spline described above is used for interpolating a one-dimensional function, where the value of the function is governed by only one variable, but in the case of a two dimensional function, we cannot use the cubic spline directly to evaluate value of the function. Rather, we must use it intelligently to interpolate a two-dimensional function. In our case, as shown in Figure 3.3, it is often necessary to find the value of a function at any point in space within the region of interest hence we need to perform a two-dimensional interpolation of the electric field, where the depth and the radius along the flaw are the two input parameters on which the function representing E depends. In two dimensions, we imagine that we are given a matrix of functional values y[j,k], where j varies from 1 to m, and k varies from 1 to n. We are also given an array x_1 of length m and an array x_2 of length n. The relation of these input quantities to an underlying function $y(x_1, x_2)$ is

$$y[j,k] = y(x_1[j], x_2[k]) \tag{3.16}$$

The basic idea of for computing two-dimensional interpolation is to divide the process into a succession of one-dimensional cubic spline interpolations. In order to do an (m-1)-order interpolation in x_1 direction and n-1 order in the x_2 direction we proceed by first locating the sub-block in which the desired point (x_1', x_2) lies, as shown in Figure 3.4. Then we compute m one-dimensional cubic spline interpolations in the x_2 direction (rows) to get function values at the points $(x_1[j], x_2)$. Finally we do a last interpolation in the x_1 direction to get the value of the function at the desired point. For performing the bicubic spline interpolation, one

calculates one-dimensional spline across the rows of the table (along the radius), followed by one additional one-dimensional splines down the newly created column (along the depth)

The value of electric field was computed at relatively few points in the region of interest in the layered sample and then using bicubic spline interpolation, we predicted the values of electric field at additional points to give a reasonably accurate value of the change in impedance of the coil. To compute the change in current in the time domain, we need to find the change in impedance at a number of frequencies. In order to reduce to computation time for calculating the change in current, we had done interpolation in frequency domain, we calculated the value of change in impedance fewer frequencies and interpolated to get values for the change in impedance at a larger number of frequencies. In this case, however, the

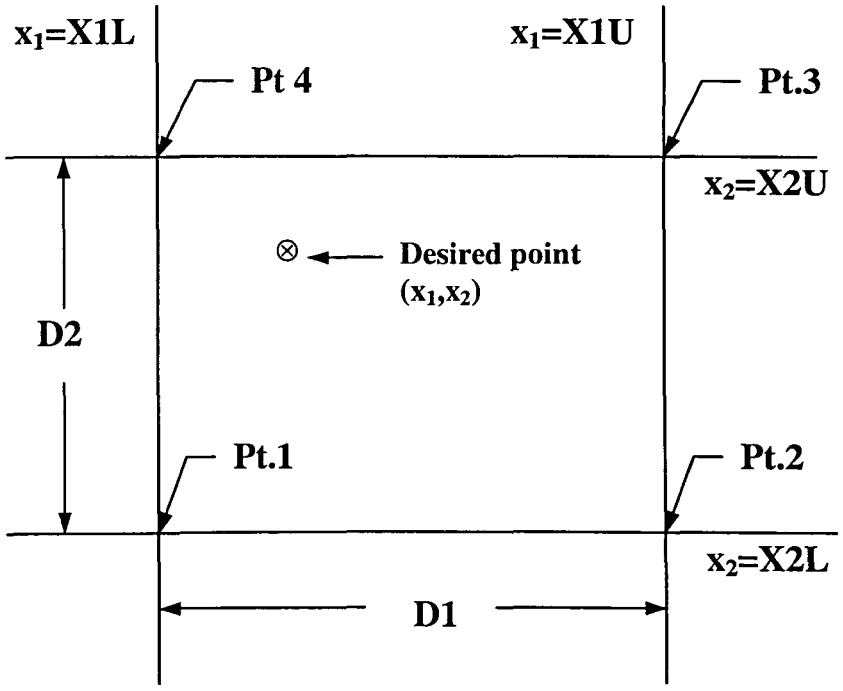

Figure 3.4: The points considered for interpolation in bicubic interpolation technique

interpolation can be nonuniform. For example in the bench mark case described later in this chapter, it was observed that the change in impedance varied rapidly in the first 50 kHz, while the change thereafter was gradual. So the change in impedance was calculated for a larger number of frequencies within the first 50 kHz and relatively fewer frequencies above 50 kHz. We then interpolated between the computed values to find the change in impedance at the desired frequency.

Using the interpolation technique the time taken to find the change in impedance at a particular frequency was reduced from three hours to ten minutes. Table 3.1 compares the computations performed using interpolation with those done without interpolation We can see that interpolation did not significantly alter the value of change in impedance. For this table the frequencies were randomly chosen and the change in impedance was computed by both methods. Figure 3.5 and Figure 3.6 show a comparison between calculated and measured values of the change in impedance with respect to frequency using the interpolation scheme. It can be seen that experiment and the calculated values are in excellent agreement.

Table 3.1: Comparison of computation with and without interpolation

Frequency (Hertz)	**Change in impedance (w/o interpolation) (ohms)**	**Change in impedance (with interpolation) (ohms)**
30555.552	0.47378 - j0.23034	0.473893 - j0.230413
40740.7382	0.346567 - j0.38778	0.346553 - j0.387836
60000.00	0.049238 - j0.457663	0.049167 - j0.457717
80000.00	0.160899 - j0.347748	0.160970 - j0.347752

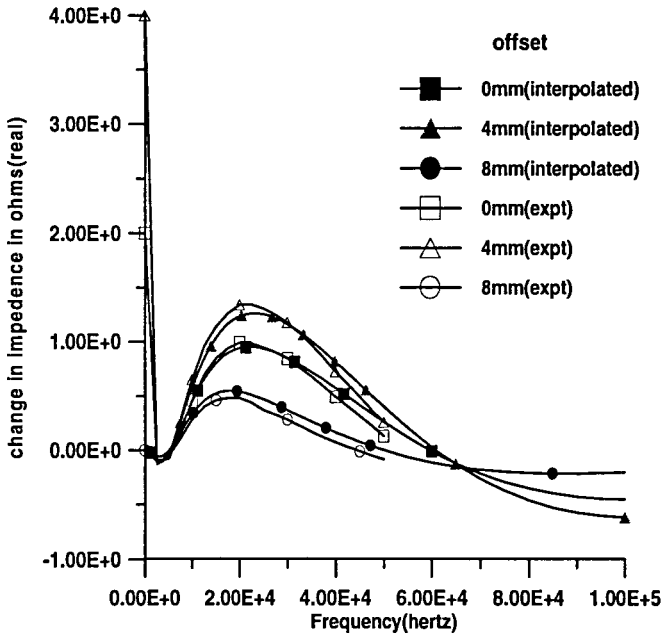

Figure 3.5: Shows the change in real part of change in impedance as function of frequency for benchmark case.

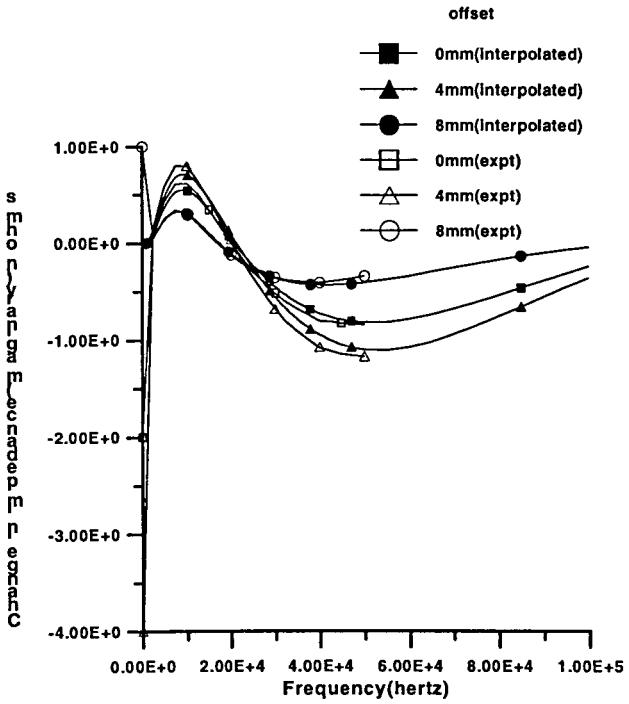

Figure 3.6: Shows the change in imaginary part of change in impedance as function of frequency for benchmark case.

3.3 Pulsed Eddy Current Measurements

As mentioned earlier, the layer approximation method provides a good estimate of the change in impedance of the coil due to a flaw in the layered surface, but the computation is very tedious.In this work we propose a method of bicubic spline interpolation to reduce the computation time. However the practical implementation of the method requires absolute measurements of the coil's impedance using a computer-controlled HP 4194A impedance analyzer, and each measurement takes approximately 150 seconds.

In this section we describe a pulsed eddy current approach for measuring the transient response of the probe due to the presence of a flaw in the layered sample that will give us information about the characteristics of the flaw. This method is significantly faster and uses less expensive equipment. Our approach is based on the pulsed eddy current equipment previously developed in our laboratories at CNDE [1]. It measures the transient voltage-current response function for step function excitation of the coil. The PC-based pulsed eddy current scanner is capable of rapid and accurate measurements, as evidenced by the good agreement obtained between theory and experiment that is shown in the results section of this chapter.

3.3.1 Theory

Consider an air-core coil placed next to a layered sample with a flaw, and it is excited by a step voltage. First, the difference between the transient current in the coil when placed next to a flawed layered sample and when placed next to a flawless layered sample is computed. The schematic diagram of the measurement is shown in Figure 3.7A, while the dimensions of the coil are shown by Figure 3.7B. The diagram shows the important

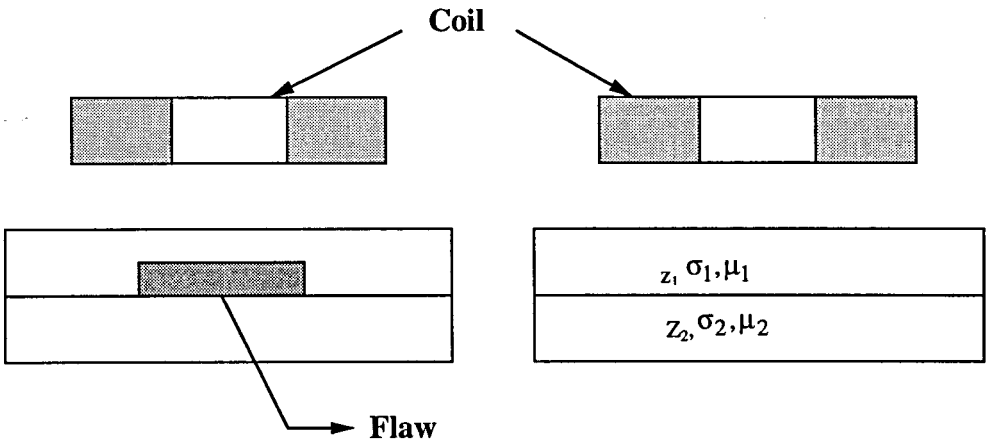

(A)

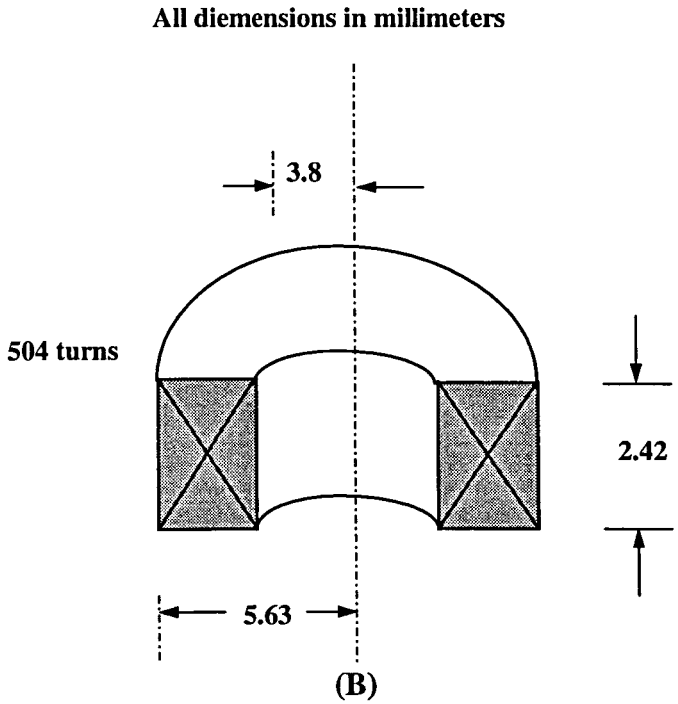

(B)

Figure 3.7: (A) Schematic representation of the experiment. (B) Geometry and dimensions of the A-probe used in the experiment.

parameters like inner radius denoted by r_1, outer radius by r_2, length of the coil (l_2-l_1), number of turns N, thickness of different layers z, conductivities and permeabilities of different layers denoted by σ and μ respectively.

The transient response of the coil is computed by first computing the change in the impedance denoted by ΔZ, of the right-cylindrical air cored eddy current coil due to the flaw in the layered metal surface using the layer approximation in the frequency domain. Then we compute the impedance of the coil when the flaw is not present in the metal, denoted by Z_0. This can be found using equation Eq. (3.17) (reviewed in [20]), which computes impedance of the probe when it is placed over a layered metal sample in the absence of the flaw.

$$Z_L = Kj\omega\int_0^{\infty}\frac{P^2(r_1,r_2)}{\alpha^5}\left\{2(l_2-l_1)+\frac{1}{\alpha}\left[2e^{-\alpha(l_1-l_2}-2+A(\alpha)\phi(\alpha)\right]\right\}d\alpha\ , \qquad (3.17)$$

where $K=\dfrac{\pi\mu_0 N^2}{(l_2-l_1)^2(r_2-r_1)^2}$,

$$P(r_1,r_2)=\int_{\alpha r_1}^{\alpha r_2} xJ_1(x)dx\,,$$

$$A(\alpha)=\left(e^{-\alpha l_1}-e^{-\alpha l_2}\right)^2,$$

$$\phi(\alpha)=\left[\frac{(\alpha+\alpha_1)((\alpha_1-\alpha_2)+(\alpha-\alpha_1)((\alpha_1+\alpha_2)e^{2\alpha_1 c}}{(\alpha-\alpha_1)((\alpha_1-\alpha_2)+(\alpha+\alpha_1)((\alpha_1+\alpha_2)e^{2\alpha_1 c}}\right].$$

The impedance of the probe when placed over a layered metal sample with a flaw present in the sample is computed as shown below.

$$\Delta Z = Z_f - Z_0\,, \qquad (3.18)$$

$$Z_f = \Delta Z + Z_0\,. \qquad (3.19)$$

where Z_f is the total impedance of the coil when placed over a layered metal sample with the flaw present in the sample. We obtain the change in admittance ΔY by taking the difference between the inverse of Z_f and the inverse of Z_0, The current difference in the frequency domain, $\Delta I(\omega)$, is found by multiplying ΔY by the input voltage V and then taking the inverse Fourier transform of $\Delta I(\omega)$ to arrive at transient response $\Delta i(t)$:

$$\Delta i(t) = IFT(\Delta I(\omega)) = \frac{1}{2\pi}\int_{-\infty}^{\infty}\frac{\Delta Y(\omega)}{i\omega}\cdot e^{i\omega t}d\omega. \tag{3.20}$$

where $\Delta I(\omega) = \Delta Y(\omega)\cdot V(\omega)$, $\Delta Y = 1/Z_f - 1/Z_0$. Furthermore $V(\omega)$ is the Fourier transform of the applied step voltage *v(t)*. Representing $\Delta Y(\omega) = R(\omega) + iX(\omega)$, we can simplify the above formula as shown below

$$\Delta i(t) = \frac{1}{\pi}\int_{0}^{\infty}\frac{R(\omega)\sin(\omega t) + X(\omega)\cos(\omega t)}{\omega}d\omega\,. \tag{3.21}$$

$\Delta i(t)$ can be compared to measurements

3.4 Experiment

All the current difference measurements were taken using the pulsed eddy current instrument diagrammed in Figure 3.8. The experimental setup of the sample was as shown in Figure 3.9. The pulsed eddy current technique excites the probe with a step voltage function, and the response of the coil when placed over a defect-free layered sample is digitized and stored as a null trace. The null trace is subracted digitally from all the subsequent responses of the coil thus finding the change in current induced in the coil. The step voltage function contains a broad range of frequencies. As a result the response over a range of frequeny can be obtained from a single step voltage function. Since the depth of penetration is dependent

on the frequency of the excitation, information over a range of depths can be obtained from a single pulse reason for which is explained in section 2.4. The pulsed eddy current instrument is a PC-based instrument and the most important components are the analog-to-digital converter, which is a 1 MHz 16-bit converter, the computer, the drive and amplifier section which drives the probe and returns the amplified signal, and lastly, the external scanner.

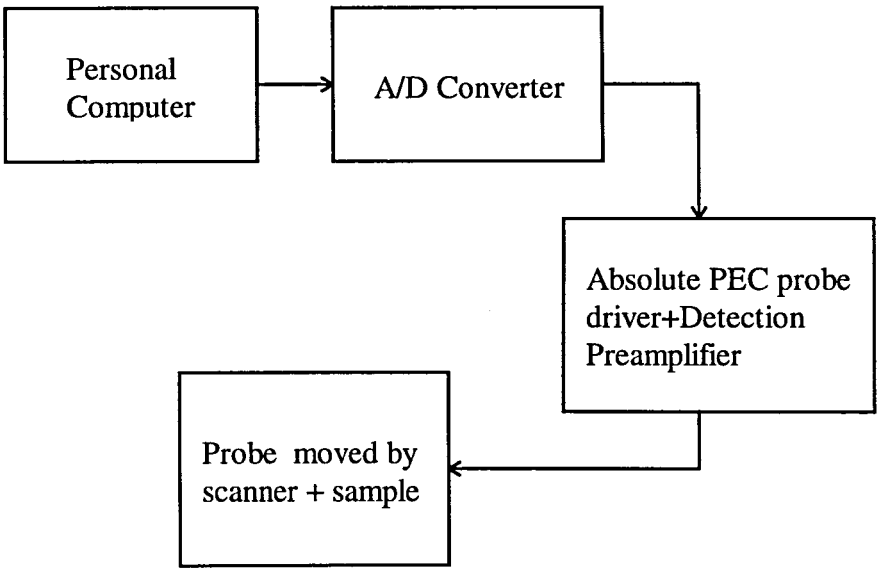

Figure 3.8: Block diagram of the pulsed eddy-current instrument used.

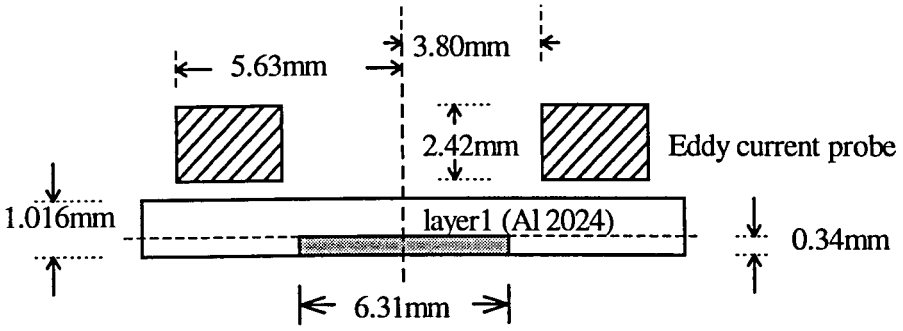

Figure 3.9: Schematic diagram of single layer of Al2024 placed under and eddy current probe with the flaw shown by the shaded area.

All measurements reported here have 500 points lying between $0\mu s$ and $499\mu s$. The probe was connected to the absolute PEC probe driver. The instrument was *nulled* by placing the coil over a presumed defect-free area of the sample. Care was taken to achieve thermal equilibrium between the coil and the sample. The sample was *scanned* by moving the probe over the entire sample to produce an image. Then the probe was moved to the defective area and the current waveform was recorded thus measuring $\Delta i(t)$, the difference of two measured currents.

The measurements were made on a 1.016 mm single layer of 2024 aluminum with a right cylindrical hole drilled on the side of the plate opposite to the coil. The change in current was measured for different offsets of the probe from the center of the flat bottom hole. Pitting corrosion in a lap joint was modeled by using two 1.58 mm sheets of 2024 aluminum, one plate laid flat on top of the other. The change in current was measured and cross-checked against theoretical results for different positions, different depths and different radii of the flat bottom hole. Table 3.2 and Table 3.3 gives the details about the sample geometry and conductivity. The coil that we used for most of the measurements is a specially wound air-core coil. Table 3.4 gives the details of the coil. The absolute PEC probe driver allows one to measure current changes in the output of a single coil.

Table 3.2: Sample geometry and conductivity of single layered sample.

conductivity of layer1	1.85×10^7 S/m (Al 2024)
thickness of layer1	1.016 mm

Table 3.3: Sample geometry and conductivity of double layered sample.

conductivity of layer1	1.85×10^7 S/m (Al 2024)
conductivity of layer2	1.85×10^7 S/m (Al 2024)
thickness of layer1	1.58 mm
thickness of layer2	1.58 mm

Table 3.4: Eddy current probe parameters (A probe).

Cross section	Right cylindrical
Number of turns	504
Inner radius	3.8 mm
Outer radius	5.635 mm
Coil height	2.42 mm
liftoff	0.229 mm

3.5 Results

3.5.1 Benchmark Problem

The benchmark problem is to determine the change in current of a right cylindrical air-core coil next to a plate that contains a right-cylindrical flat bottom hole on the side opposite to the coil. The test sample as shown in Figure 3.9 consists of a single 1-mm thick plate of 2024 aluminum alloy with conductivity of 1.85×10^7 S/m. A right-cylindrical hole was drilled on the side of the plate opposite to the coil. The diameter of the hole was 6.31 mm and average depth of this flat bottom hole was 0.34 mm. Figure 3.10 shows the theoretical (smooth curve) and experimental values for the change in current induced in the coil when it was placed at two different positions. First when the center of the coil was directly above the center of the flaw (offset of 0 mm). Second when the center of the coil was offset from the center of the flaw (offset of 3.15 mm).We see that the change in current was

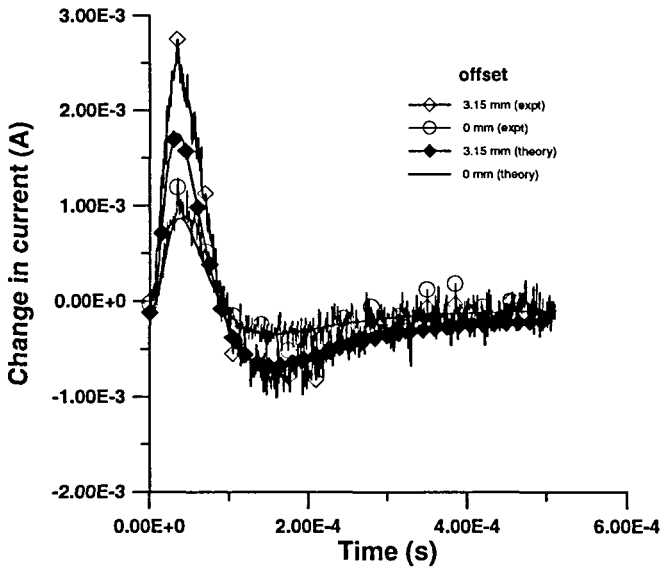

Figure 3.10: Shows the change in current in coil for its different offsets when placed over a single Al2024 layer with flaw on the bottom.

smaller at the center and larger at the edges of the flaw. Actually when the coil which is placed far away from the flaw and is brought slowly nearer to the flaw, we see a gradual increase in the change in current with peak reaching maximum when the center is over the edge of the flaw and the change in current decreases as the coil moves from edge of the flaw to center. The current induced in the metal and the degree to which it is diverted is the key to understanding the behavior of the change in current. The signal is cylindrically symmetric, since the coil and defect are also cylindrically symmetric. The induced current is the shape of a ring with current being strongest directly beneath the wires of the coil. The induced current is zero at the center of the coil and also decays external to the coil. So when the flaw is located either at the center of the coil or away from the coil the deflection of the current due to the flaw is relatively smaller than the deflection of the current when the coil is placed at

the edge of the flaw. Hence the change in current in Figure 3.10 is greatest when the coil is on the edge of the flaw.

3.5.2 Pitting Corrosion in a Lap Joint

Two 1 mm thick sheets of 2024 aluminum, one plate on top of other as shown in Figure 3.11, are used to model a lap joint. The conductivity of the sheets was assumed to have an uniform value of 1.85×10^7 S/m and the flaw was modeled as flat bottom hole. The change in current in the coil was analyzed for different depths, different positions and different radii of the flat bottom hole. Qualitatively, the shape of the curves is similar to that observed in the case of the single layered benchmark case, but the major difference is that the signal was reduced by a factor of two for the lap-joint geometry. experimental results for the change in current in the coil as a function of time due to a flaw is that a right cylindrical flat bottom hole located at the bottom of the top layer of the two- layered sample. The comparison was made for flaws of radii 3.12 mm and 9.42 mm. The Figure 3.12 shows the comparison between theoretical (smooth curve) and

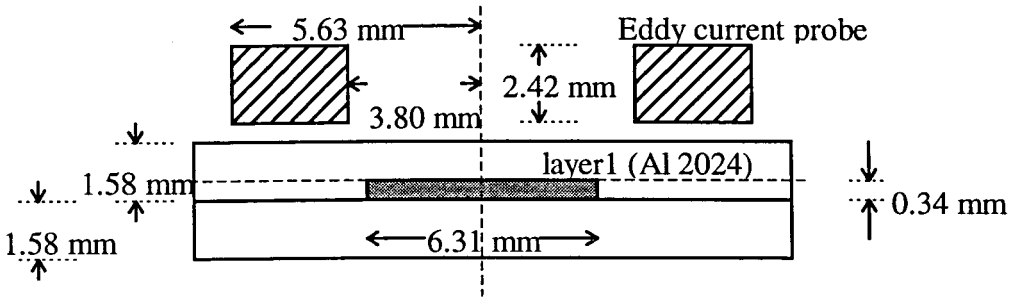

Figure 3.11: Schematic diagram of lap-joint sample modeled by placing one Al2024 sheet on an other. Flaw is located at the bottom of the top layer shown by shaded region.

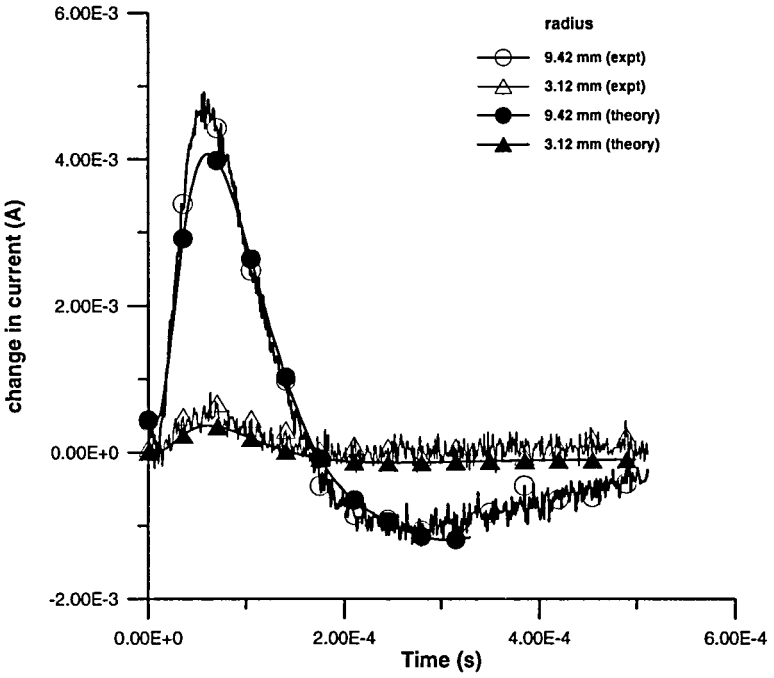

Figure 3.12: Shows the change in current in coil as a function of time, for different flaw radius, for a lap-joint sample.

current change predicted, as can be seen, is in good qualitative agreement with the practical measurements made.

The variation of the peak amplitude of the signal with the increase in radius of the flaw is shown in Figure 3.13. We can see that initially the signal increases gradually and there is a significant change in the rate of increase when flaw the radius equals the innerradius of the coil. As flaw radius continues to increase the increase, the signla gradually increases and flattens out.

Figure 3.14 shows a comparison of the change in current induced in the coil as a function of time due to 10%, 20% and 30% flaws, where the flaw is a right cylindrical flat

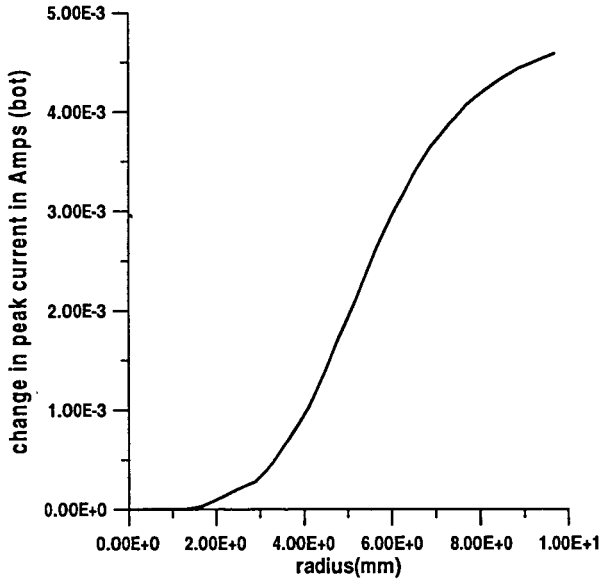

Figure 3.13: Shows the variation of the peak amplitude of change in current as function of radius of the flaw at the bottom of the top layer in lap-joint sample.

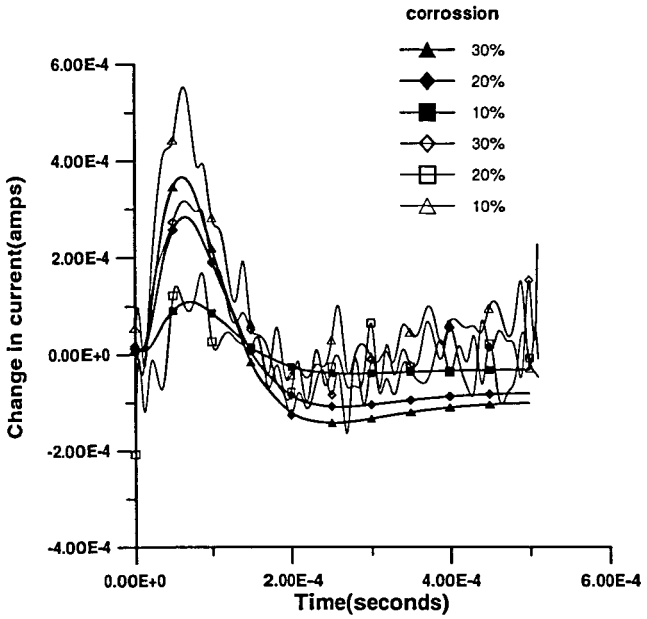

Figure 3.14: Shows the variation of change in current in the coil for different amounts of corrosion for the flaw at bottom of the top layer in lap-joint sample.

bottom hole and the flaw is at the bottom of the top layer of the two layered sample. We can see that the peak of the signal increases with the increase in amount of corrosion this is explained by the fact that the greater the loss of metal, the greater is the deviation of eddy currents in that area. We can also observe from the plots that the zero-crossing time increases with decreasing amounts of corrosion.

Figure 3.15 shows the change in current induced in the coil for different positions of the flaw: bottom of top layer, top of bottom layer and bottom of bottom layer. The flaw in this case was a flat bottom hole of radius 3.1 mm and modeled 30% pitting corrosion in the lap joint. The peak of the change in current decreased as the flaw moved farther away from the coil. The peak-arrival time and zero-crossing time increased as the distance of the flaw from the coil increased. Figure 3.16, Figure 3.17 and Figure 3.18 show the comparison of experimental and theoritical results for the same three cases.

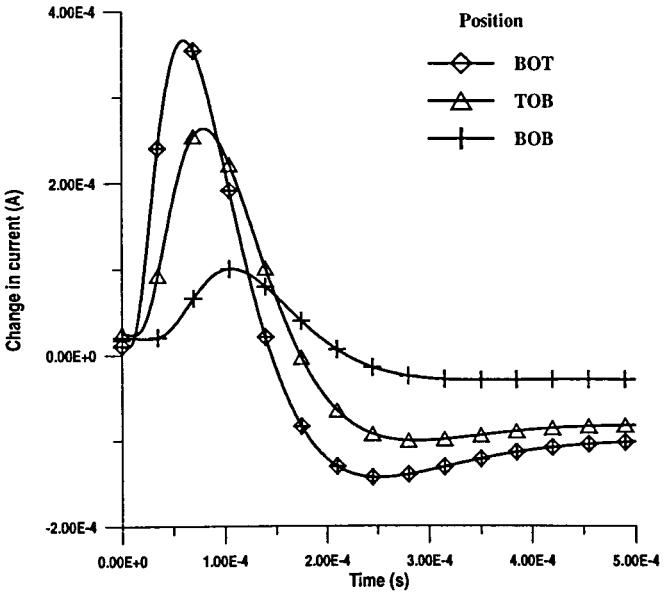

Figure 3.15: Shows the change in current for different position of flaw in the lap-joint

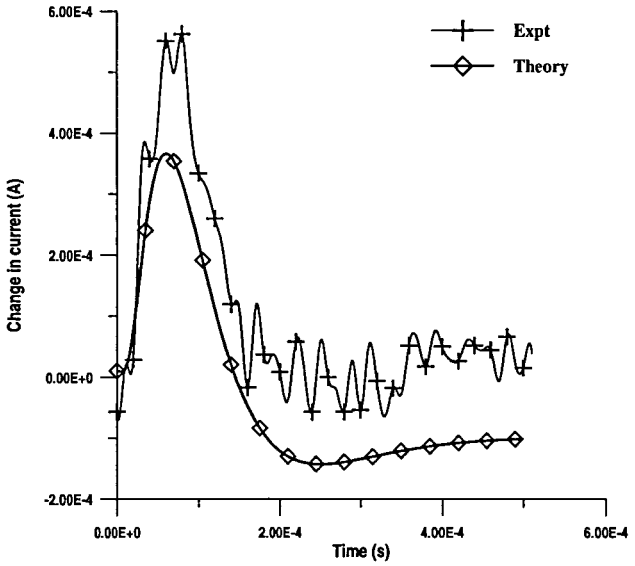

Figure 3.16: Validation of calculated change in current when the flaw is at top of the bottom layer

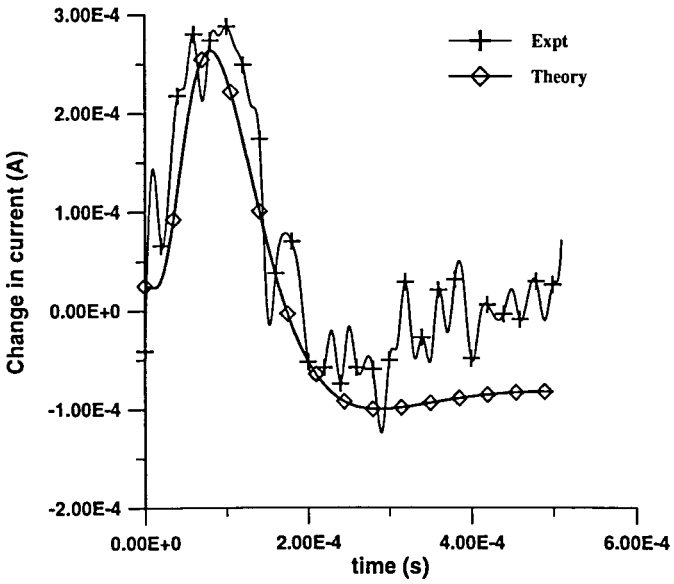

Figure 3.17: Validation of calculated change in current when the flaw is at bottom of top layer

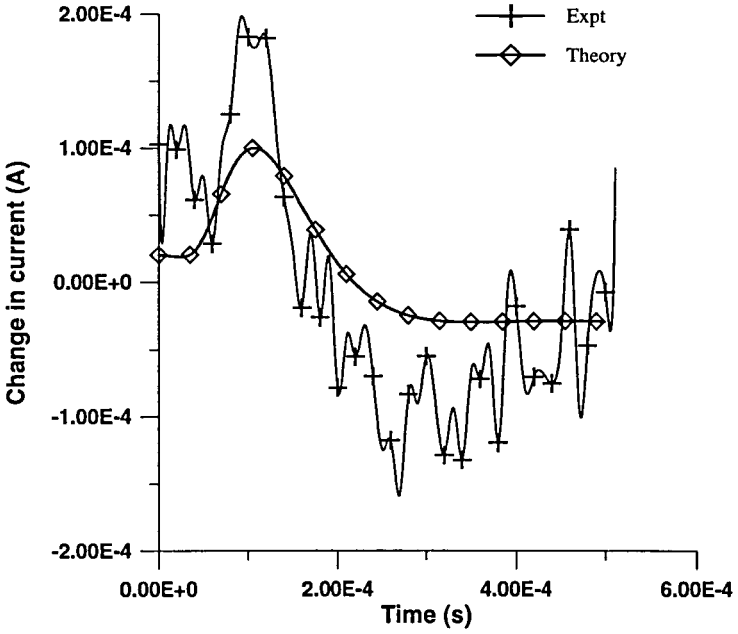

Figure 3.18: Validation of calculated change in current when the flaw is at bottom of the bottom layer

3.6 Summary

We have proposed a faster approach to solve the forward problem of pulsed eddy current characterization of corrosion-induced loss of metal in aircraft structures. Compared to the previously developed swept frequency method (layer approximation), the method proposed hence is much faster and simpler and the equipment used is less expensive and portable. Using the layer approximation technique, which calculates change in impedance induced by a three-dimensional defect in layered metallic structure we found the change in current induced in the coil excited by pulsed signal. Using the technique of interpolation, the execution time of the code for computing the change in impedance using layer approximation

was reduced significantly. First the electric field values in the region of interest were interpolated and then the change in impedance at various frequencies were interpolated, thus reducing the number of complex and time consuming calculations. The change in current as a function of time was computed for a single layered sample and also for flaws in lap-joints. Also we computed signals for various positions and sizes of flaws. The most advantageous aspect of this approach is that it can compute the change in current for the case of flaws smaller than the probe. Finally the computed results were compared with experiment.

4. PULSED EDDY CURRENT TECHNIQUE FOR DETECTION OF CRACKS

Some of the main type of flaws found in metallic structures are corrosion and cracks. In chapter 3 we described efficient methods to solve the forward problem by finding the change in impedance of the probe when placed over a flat bottom hole, which is a reference sample analogous to pitting corrosion. But the method described in chapter 3 cannot be applied to find the solution of the forward problem for a defect like a fatigue crack, which constitutes an important class of flaws for eddy current testing. This chapter applies the Fourier transform method described in the Chapter 3 to the frequency domain solution obtained for cracks developed by Nakagawa [3]. This chapter gives a brief overview of Nakagawa's approach and then presents the pulsed eddy current implementation of the solution, followed by results.

4.1 Theory

The flaw and the sample which are to be studied in this chapter are shown in Figure 4.1. In order to explain the concepts involved, the sample is a metal specimen with a flat surface and we consider a surface-breaking flaw denoted by S_c on the flat surface, which is denoted by S_f. Here the flaw is a tightly closed crack, i.e. a crack with infinitesimally small width. The sample was scanned by an EC probe, the probe was assumed to be a cylindrical, air-core coil, placed parallel to the surface.

We proceed with the theoretical formulation by first obtaining the electromagnetic field configuration by solving Maxwell's equations. Here we use the boundary integral equation (BIE) method [21,22]. We use this method because it reduces the number of

unknowns, hence it reduces the computational complexity. The quasi-static assumption further reduces the complexity.

The flaw is considered as tightly closed hence this reduces the computational tasks further. When the crack is tight, a potential method introduced by Bowler [23,24] can be used. First let us define a tight crack: it is defined as the limit of an open crack where the two sides approach each other but remain separated by infinitesimal distance. Let S_c be the single limiting surface of the two approaching surfaces. Let $disc\overline{H}$ denote the discontinuity of the magnetic field $\overline{H}$ across S_c. It turns out that on the crack surface, only a single scalar

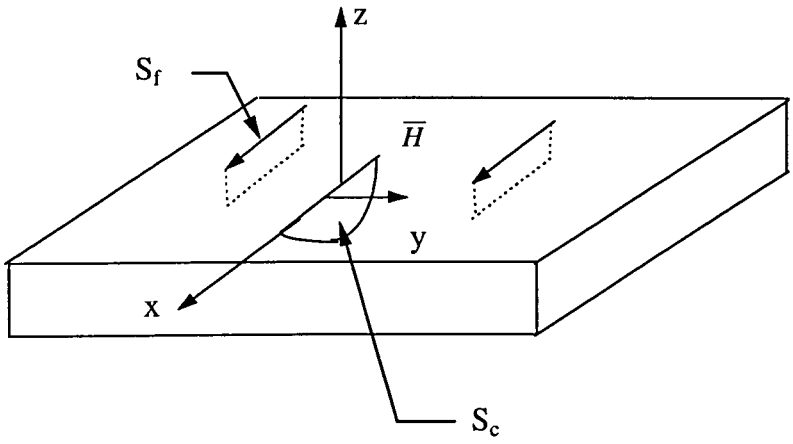

Figure 4.1: An eddy current probe scanning over a flat surface S_f of a metal specimen occupying the halfspace, giving uniform magnetic field over the surface. The S_c denotes the face of the crack

function (denoted by ϕ) defined on S_c remains independent. Namely, only the tangential components of E are discontinuous across S_c, and expressed as

$$disc\overline{E}_t = -\overline{\nabla}_t \phi. \qquad (4.1)$$

The Eq (4.1) is valid only on crack surfaces S_c, and is derived from $disc\overline{H} = 0$ and Maxwell's equations. This reduces the number of independent degrees of freedom and hence makes the tight crack problem tractable. From the study done by Bowler on a subsurface crack we can know that the potential ϕ is constant along the edge of the crack, which can be set to zero by definition. When considering the boundary conditions at the mouth of the crack, the fluid flow analogy is used. In this analogy, eddy current flow is regarded as fluid flow. And the mouth region of the crack becomes the stagnation point at which the flow velocity vanishes. Hence, from this analogy we can assume that $\partial_n \phi$ of the potential should vanish on the mouth of the crack, as shown schematically in Figure 4.2.

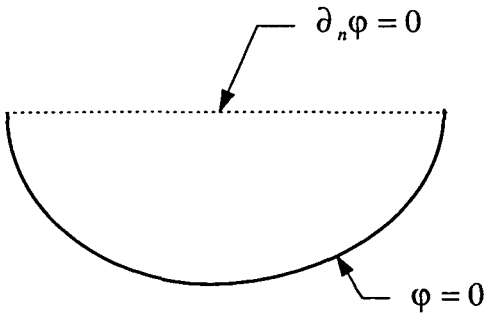

Figure 4.2 : The boundary conditions satisfied by the Bowler potential.

From the studies of BIEs, a set of integral equations is derived to evaluate ϕ . From two dimensional Poisson equation on S_c,

$$\Delta^{(2)}\phi = -\Phi \tag{4.2}$$

with a source term Φ.

Writing Green's formula written for E_y inside the metal

$$E_y^{(0)}(x,0,z) = \int_{S_c} dx'dz'K(x,z;x',z')\Phi(x',z'), \tag{4.3}$$

where $\sigma E_y^{(0)}$ is the incident eddy current density in the absence of the flaw, and the kernel K can be obtained from the BIEs after eliminating the S_f variables,

From Eq. (4.2) and the boundary condition, the normal derivative of $\partial_n\phi$ can be obtained from the BIE.

$$\phi^{(0)}(x,z) = -\int_c dsg(x,z;x(s),z(s))\partial_n\phi(s) \tag{4.5}$$

where C is the contour representing the bottom edge and where

$$\phi^{(0)} = \int g\Phi, g(x,z;x',z') = -(1/4\pi)\ln\{(x-x')^2 + (z-z')^2\}; \qquad (z' \to -z') \tag{4.6}$$

From the solution of Eq. (4.3) and Eq. (4.5), the impedance changes can be finally calculated by

$$\Delta Z = \left(\frac{\sigma}{I^2}\right)\int_{S_c} \phi E_y^{(0)} \tag{4.7}$$

The real cracks does not have zero width therefore to compensate for the effect of volume of the void in the crack due to the width a constant is added to the change in impedance to arrive at the actual change in impedance in case of real cracks. The specimen goemetry can be either half space or plate, with an appropriate choice of the kernel K in Eq. (4.3).

The pulsed eddy current implementation involves calculating ΔZ assuming the probe is normal to the surface and then finding the change in admittance ΔY given by the relation

$$\Delta Y = \frac{1}{\Delta Z + Z_0} - \frac{1}{Z_0} \tag{4.8}$$

where Z_0 is the probe impedance on the flawless metal surface. Following the procedure described earlier in Chapter 3 the transient response of the step voltage applied can be calculated by Fourier transformation of $\Delta Z(f_i)$.

4.3 Results

The problem is to determine the transient response of the right cylindrical air-core coil placed next to a plate sample containing a crack-like defect. The position of the defect can either be on the side opposite to the coil or on the same side as the probe. The experimental setup is as shown in Figure 4.3. The test sample is a single 0.935 mm thick plate of 2024. aluminum alloy with conductivity of 1.615×10^7 S/m. A rectangular EDM notch is made tosimulate a fatigue crack. The dimensions of the defects to be considered are su mmarized in

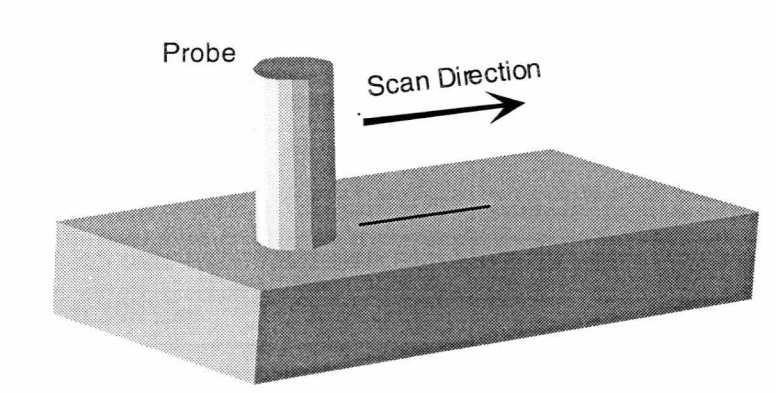

Figure 4.3: Experimental setup for detection of cracks

Table 4.1 and that of the probes in Table 4.2. The defects being considered can be mainly divided into two classes: those whose length is greater than the diameter of the probe and other whose length is less than the diameter of the probe. Let us pause for a moment and study the behavior of the change in impedance of a coil when the coil moves along the length of the flaw [25]. Figure 4.4A and B show the variation of ΔZ when the probe moves along the crack. In first case the length of the flaw is greater than that of the diameter of the probe as shown in Figure 4.4A. In this case as the probe moves in from the left the ΔZ response

Table 4.1: Parameters of A-probe and 1107 probe.

Specifications	A-probe	1107-probe
No of turns	504	200
Inner radius	3.8 mm	2.55 mm
Outer radius	5.63 mm	4.61 mm
Height	2.64 mm	1.55 mm
Built-in liftoff	0.0 mm	0.0 mm
External liftoff	0.178 mm	0.133 mm

Table 4.2: Parameters of the flaw samples used for computations

Specifications	Flaw1	Flaw2	Flaw3	Flaw4
Material	Al-2024	Al-2024	Al-2024	Al-2024
Conductivity	1.615E7 S/m	1.615E7 S/m	1.615E7 S/m	1.615E7 S/m
Length	3.5 mm	7.0 mm	14.35 mm	22.6 mm
Width	0.198 mm	0.361 mm	0.227 mm	0.257 mm
Depth	0.485 mm	0.515 mm	0.447 mm	0.496 mm
Shape	Rectangular	Rectangular	Rectangular	Rectangular
Thickness of	0.935 mm	0.935 mm	0.935 mm	0.935 mm

increases when the flaw begins to intercept the current loops. This continues till the dead spot (center of the probe) reaches the end of the flaw. Near this point in the scan the probe can no longer sense the end of the flaw, and a flat spot occurs in the flaw profile. The ΔZ response increases again as the probe moves further onto the flaw, and then it flattens out when the eddy current pattern moves entirely onto the central part of the flaw. In this region the probe does not sense the ends of the flaw and the response is independent of the position. The same sequence repeats in reverse order at the other end of the flaw. In the second case, when the flaw is much smaller than the probe the ΔZ response is as shown in Figure 4.4B. In this case the flaw does not extend over more than a small part of the eddy current pattern. Instead the entire flaw lies in the dead spot when probe is centered on the flaw. Thus a flaw profile in this case will have two peaks. Typical plots for 7 mm flaw and 14 mm flaw with the defect on the same side of the sample as the probe is shown in Figure 4.5 and Figure 4.6. We can observe similar patterns explained earlier for the two types of flaws.

4.3.1 Flaws at the Front Side

First let us consider the flaws on the front side, i.e., when the flaw is on the same side as the probe, as shown in Figure 4.7. Here we considered four samples with flaw lengths 3.5 mm, 7 mm, 14.35 mm and 22.3 mm and probe designated as 1107, whose dimensions are listed in Table 4.2. The experiment was performed in a similar procedure as that explained in Chapter 3. The behavior of the peak value of the transient current response is similar to the behavior of ΔZ explained above when the probe is moved along the flaw. The transient current responses shown in Figure 4.8, Figure 4.9 and Figure 4.10 are computed at the position of the probe on the crack where ΔZ is maximum hence from earlier explanation for

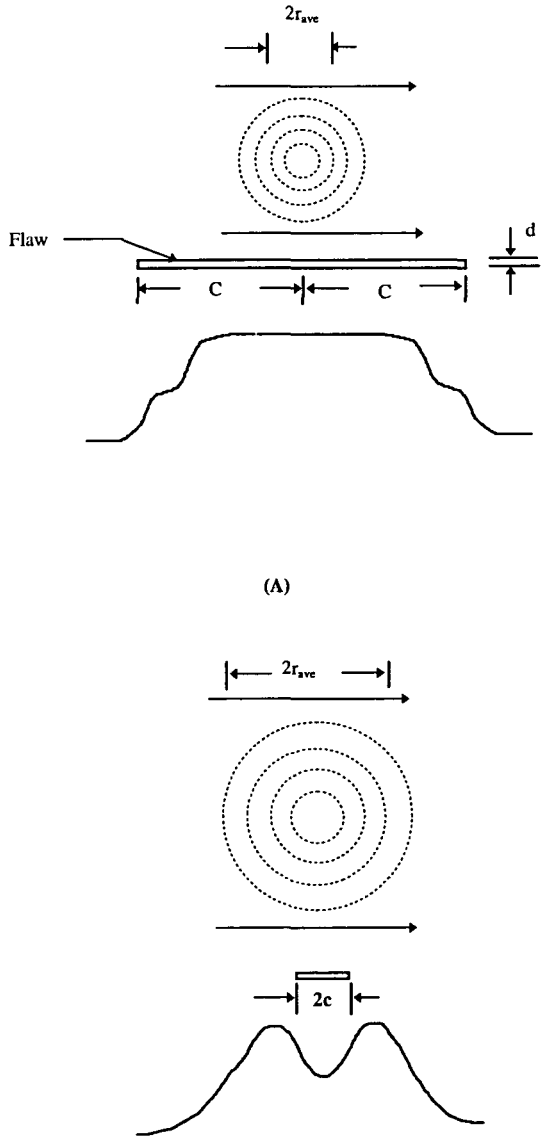

Figure 4.4: Schematic showing the variation of change in impedance of the probe when it moves along the length of the flaw (A) Flaw length smaller than that of the average diameter of the probe (B) Flaw length is greater than the average diameter of the probe [25].

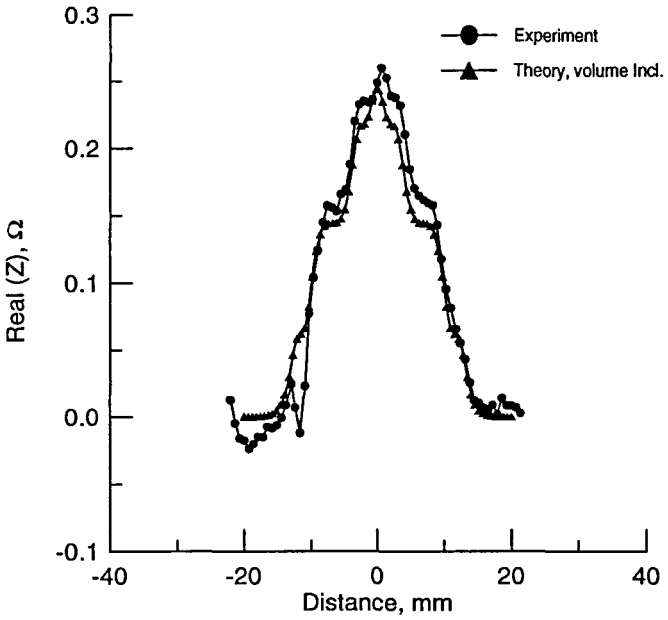

Figure 4.5: The real part of change in impedance when the A-probe is moved along the 14 mm flaw. This is a typical case when the flaw is bigger than the probe.

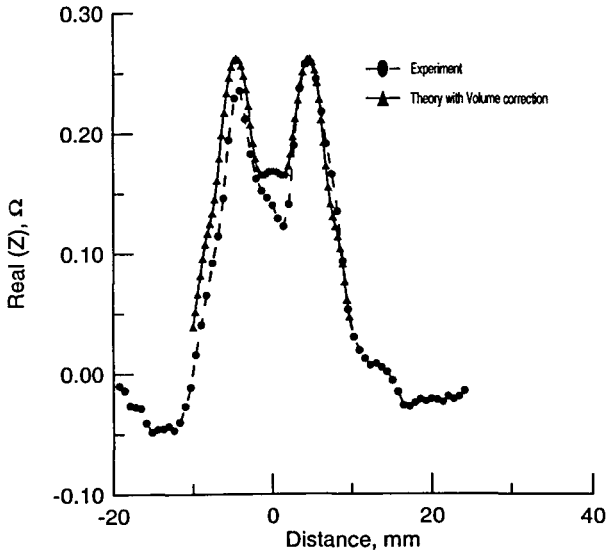

Figure 4.6: The real part of change in impedance when the A-probe is moved along the 7 mm flaw. This is a typical case when the flaw is smaller than the probe.

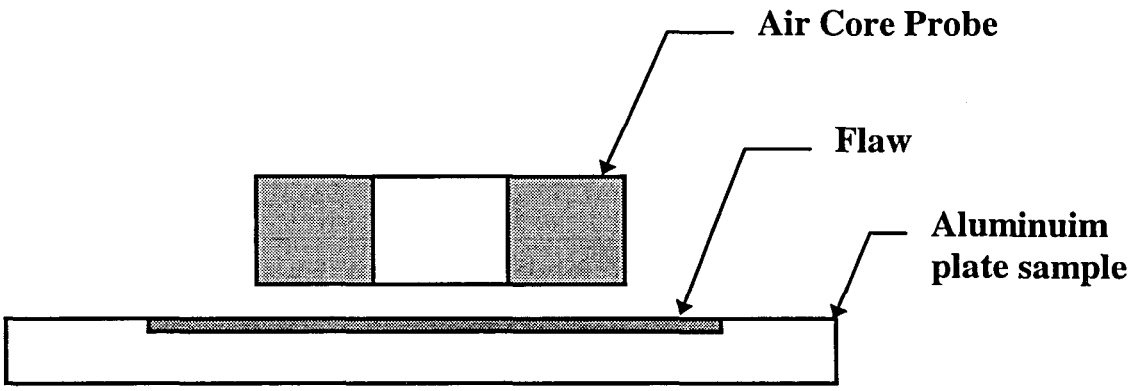

Figure 4.7: Schematic diagram showing the flaw on the front side of the plate.

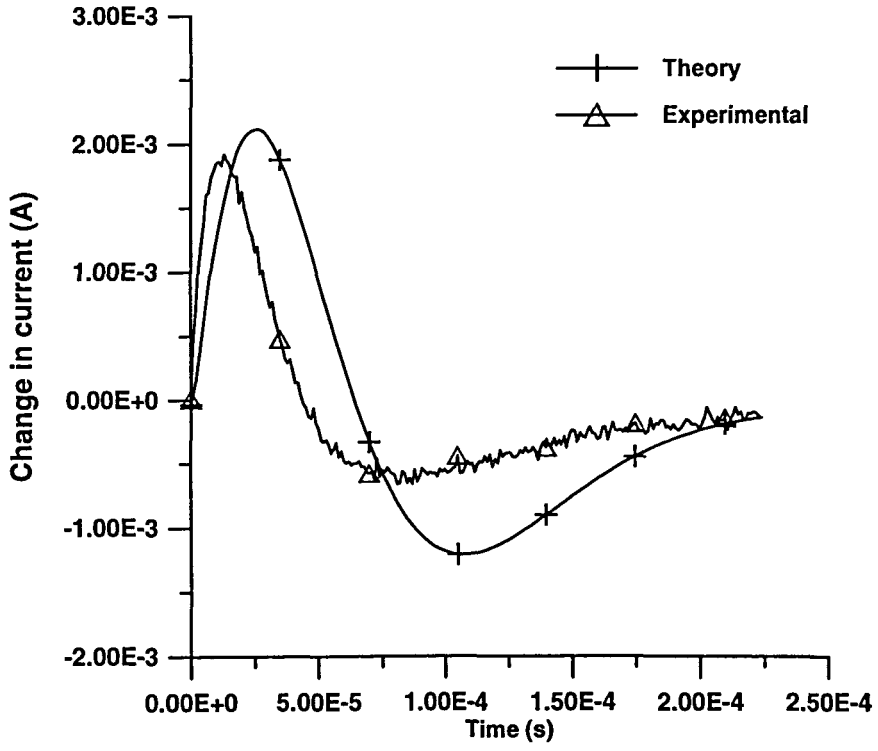

Figure 4.8: Transient response of probe 1107 when placed on 3.5 mm flaw on front side.

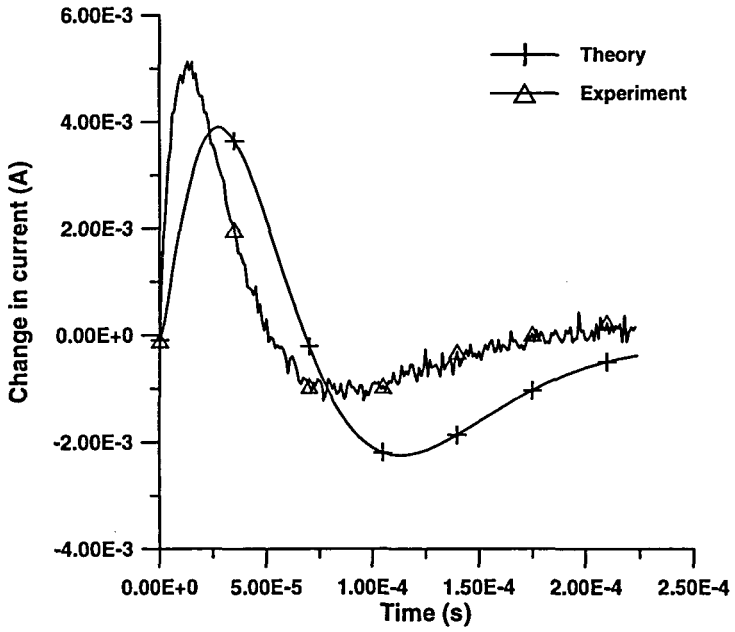

Figure 4.9: Transient response of probe 1107 when placed on 7.0 mm flaw on front side

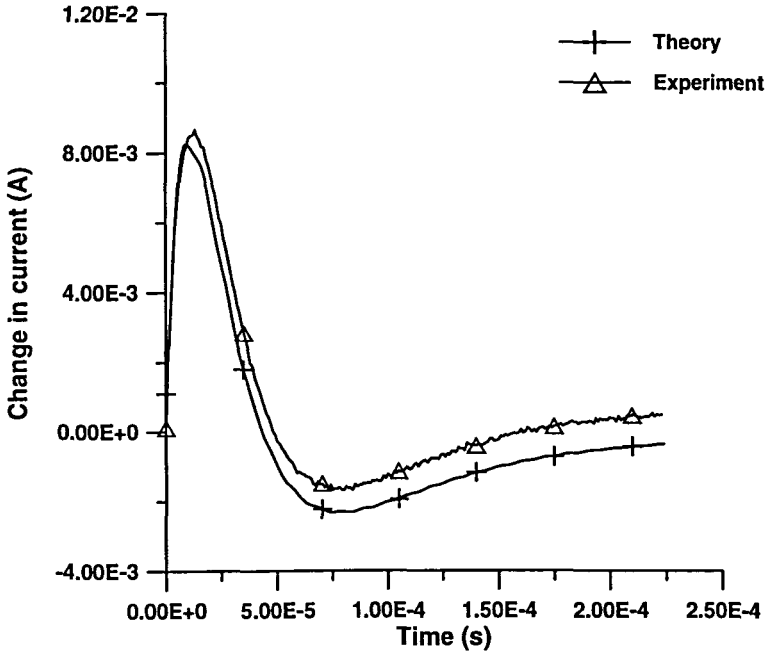

Figure 4.10: Transient response of probe 1107 when placed on 14.35 mm flaw on front side of the plate sample.

the 14 mm flaw the transient current response was measured at the center of the crack, whereas for 3.5 mm and 7 mm cracks the probe was offset. We can see in Figures 4.8-4.10 that we have a reasonably good agreement between theory and the experiment, especially the amplitude of the peak in the waveform.

4.3.2 Flaw on the Back side

Now let us consider flaws on the back side of the plate sample, as shown in Figure 4.11. The same samples are taken and the experiment done for the front side is repeated. Their transient response is shown in Figure 4.12 , Figure 4.13 and Figure 4.14, for 3.5 mm, 7.0 mm and 14.35 mm cracks, respectively. Again we can see that the theory and experiment agree reasonably well.

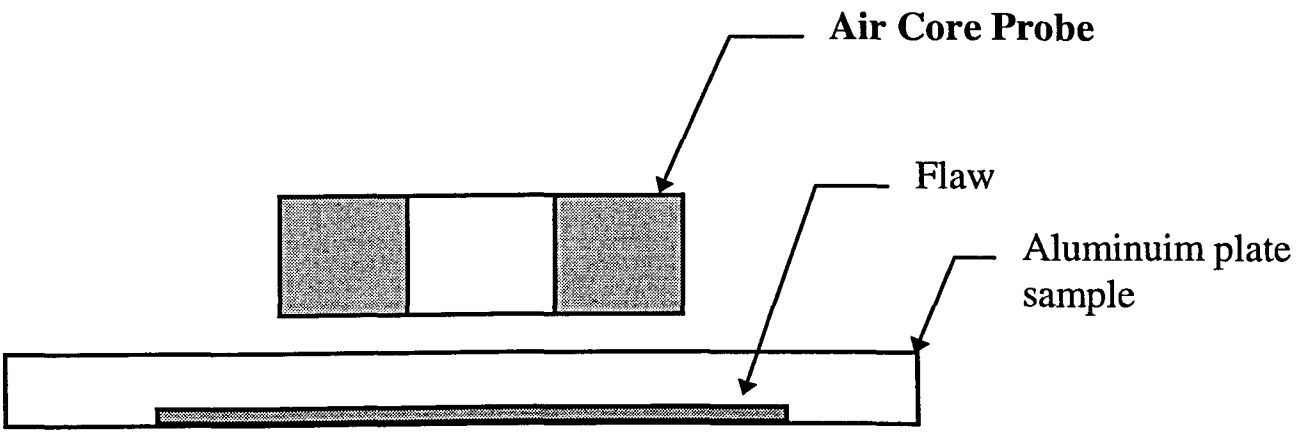

Figure 4.11: Schematic diagram showing the flaw on the back side of the plate sample.

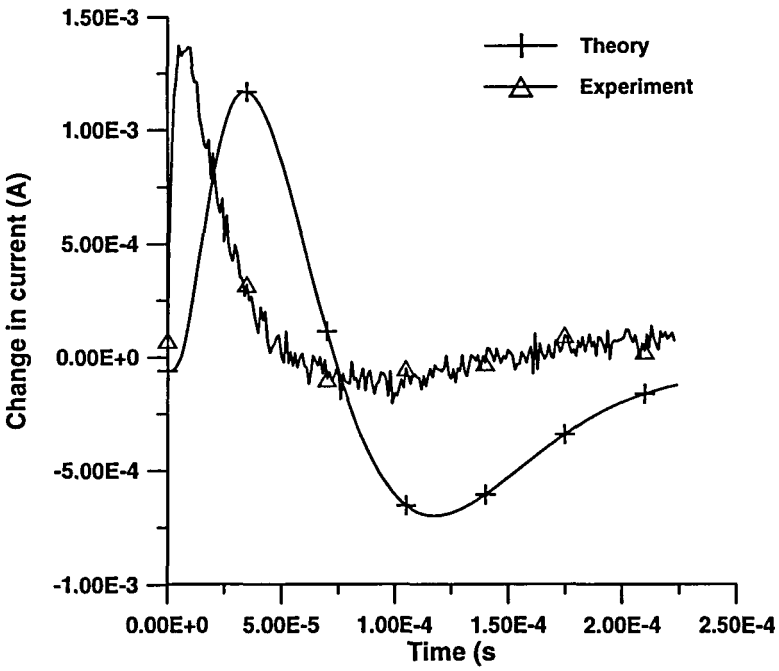

Figure 4.12: Transient response of probe 1107 with 3.5 mm flaw on back side of the plate sample.

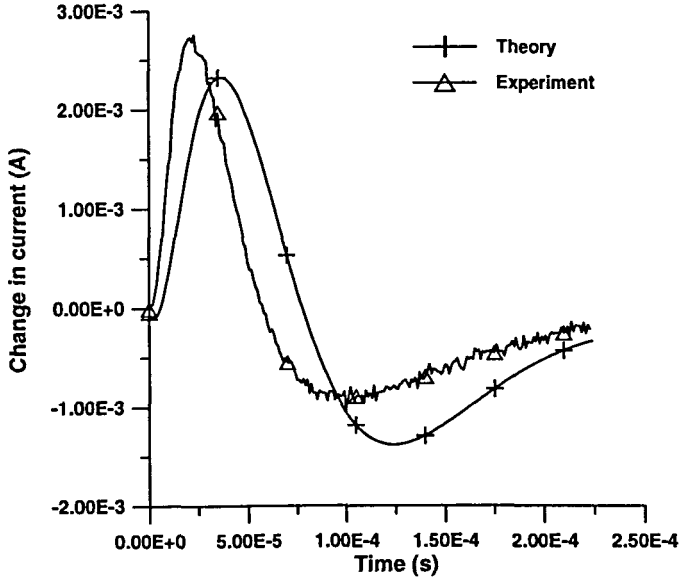

Figure 4.13: Transient response of Probe1107 with 7.0 mm flaw on back side of plate sample.

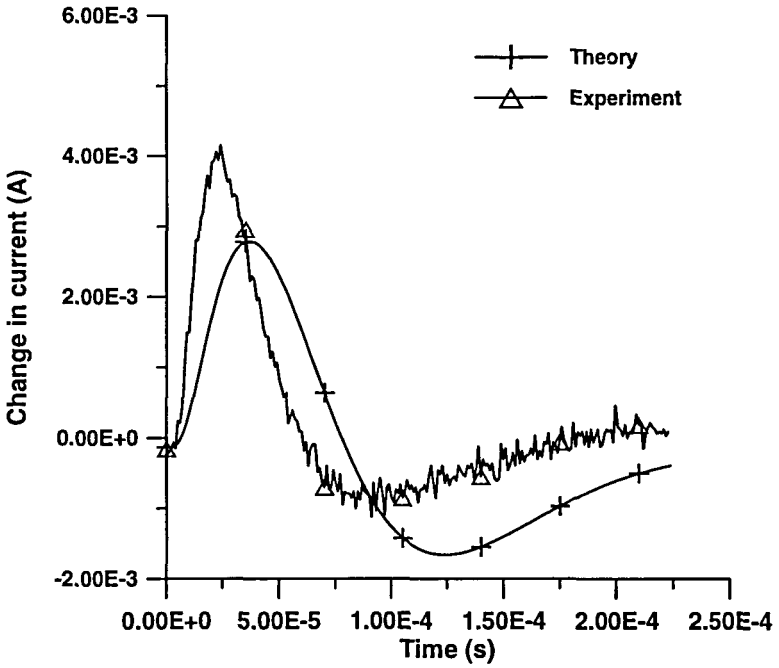

Figure 4.14: Transient response of Probe 1107 with 14.3 mm flaw on back side of plate sample.

5. SUMMARY AND CONCLUSIONS

After many years of service an aircraft will reach an age where fatigue cracks and corrosion develop, causing deterioration in structure and also affecting the safety of its usage. Hence there is a need for efficient, less expensive techniques to detect the fatigue cracks and corrosion. In this thesis we have proposed and demonstrated pulsed eddy current based techniques for detection of both fatigue cracks and corrosion. Compared with the previously developed swept frequency technique, the present approach is simpler, faster and the pulsed eddy current equipment developed at CNDE for defect detection is less expensive and easily portable. We developed a theoretical model for pulsed eddy current measurements and the model showed good agreement between experiment and theory.

We used a layer approximation technique as the basis for developing the theoretical model for detection of corrosion. This technique is used to calculate the change in impedance induced by a three-dimensional defect in layered metallic structures. Using this information we found the change in current induced in a coil excited by step change of voltage when the coil is placed over a defective sample. But the layer approximation technique involves time consuming computations. By using the technique of interpolation, the computation time of the technique was reduced. First the electric field values in the region of interest were interpolated and then change in impedance at various frequencies were interpolated, thus reducing the number of complex and time consuming calculations. The change in current as a function of time was computed for single-layered sample and also for flaws in lap-joints. We also calculated signals for various positions and sizes of the flaws. The most advantageous

aspect of this approach is that it can also compute the change in current for the case of flaws smaller than the probe.

We used the boundary integral equation based method as the basis for developing the theoretical model for detection of cracks. The BIE technique was used to compute the change in impedance of the probe when placed on a crack-like defect. Using this information the change in current was computed. We made experimental measurements on four samples containing EDM notches used for simulating real cracks. These samples included both cracks which are smaller and larger than the probe diameter. The computations and the measurements were carried out for both cases of cracks on both front and back sides of the sample. Again, as with the calculations for corrossion-like defects, the results comparing calculated signals with measurements showed good agreement.

BIBLIOGRAPHY

[1] J. C. Moulder , M. W. Kubovich, E. Uzal, J. H. Rose, "Pulsed eddy-current measurements of corrosion-induced metal loss: Theory and experiment", Review of Progress in Quantitative Nondestructive Evaluation, Edited by D. O. Thompson, D. E. Chementi, Vol. 14, Plenum Press, New York, p. 2065 (1995).

[2] R. Satveli, J. C. Moulder, J. H. Rose, "Impedance of a coil near an imperfectly layered metal structure: The layer approximation", Journal for Applied Physics, Vol. 79, p. 2811 (1995).

[3] N. Nakagawa, "Eddy-current detection methods for surface-breaking tight cracks", Review of Progress in Quantitative NDE, edited by D. O. Thompson and D.E. Chimenti, Vol. 8A, Plenum Press, New York, p. 245 (1989).

[4] J. H. Rose, E. Uzal, J. C. Moulder, "Pulsed eddy-current characterization of corrosion in aircraft lap-splices", SPIE, Vol. 2160, p. 164 (1993).

[5] J. R. Bowler, D. J. Harrison, "Measurement and calculation of transient eddy-currents in layered structures", Review of Progress in Quantitative NDE, edited by D. O. Thompson and D. E. Chimenti, Vol. 11, Plenum Press, New York, p. 241 (1992).

[6] R. E. Beissner, J. L. Fisher, "A model of pulsed eddy current detection", Review of Progress in Quantitative NDE, edited by D. O. Thompson and D. E. Chimenti, Vol. 5, Plenum Press, New York, p.189 (1986).

[7] J. L. Fisher, R. E. Beissner, "Pulsed eddy-current crack-characterizing experiments", Review of Progress in Quantitative NDE, edited by D. O. Thompson and D. E. Chimenti, Vol. 5, Plenum Press, New York, p.199 (1986).

[8] C. V. Dodd and W. E. Deeds, "Analytical solutions to eddy-current probe-coil problems", Journal for Applied Physics, Vol. 39, p. 2829 (1968).

[9] C. C. Cheng,C. V. Dodd and W. E. Deeds, "Analytical solutions to eddy-current probe-coil problems over layered metals" International Journal for Nondestrucive testing, Vol. 109, p. 90 (1969).

[10] B. Hull, V. John, *Non-Destructive Testing*, Macmillan Education, London (1988).

[11] David H. S. Cheng, "The reflected impedance of a circular coil in the proximity of a semi-infinite medium", IEEE Transaction for Instrumentation and Measurements, Vol. 14, p.107 (1965).

[12] S. M. Nair and J. H. Rose, "Reconstruction of three-dimensional conductivity variations from eddy current data", Inverse Problems, Vol. 6, p.1007 (1990).

[13] S. M. Nair and J. H. Rose "Low frequency asymptotic for eddy currents in a conductivity halfspace in the absence and presence of inhomogeneties", Journal for Applied Physics, Vol 70, p. 1170 (1991).

[14] B. A. Auld, *Eddy-current characterization of materials and structures*, edited by G. Birnbaum and G. Free, American Society for Testing and Materials, Philadelphia (1981).

[15] B. A. Auld, S. R. Jefferies and J. C. Moulder. "Eddy-current signal analysis and inversion for semielliptical surface cracks", Journal for Nondestructive Evaluation, Vol. 67, p. 1140 (1988).

[16] N. Nakagawa, S. Mitra and J. C. Moulder, "Eddy-current corner crack inspection", Review of Progress in Quantitative NDE, edited by D. O. Thompson and D. E. Chimenti, Vol. 11A, Plenum Press, New York, p. 233 (1992).

[17] N. Nakagawa and J. C. Moulder, "A model of bolt hole inspection via eddy currrent", Review of Progress in Quantitative NDE, edited by D. O. Thompson and D. E. Chimenti, Vol. 12A, Plenum Press, New York, p. 259 (1993).

[18] S. Mitra, P. Urali, E. Uzal, J. H. Rose and J. C. Moulder, "Eddy-current measurements of corrossion-related thinning in aluminum lap-splices", Review of Progress in Quantitative NDE, edited by D. O. Thompson and D. E. Chimenti, Vol. 12, Plenum Press, New York, p. 2003 (1993).

[19] W. H. Press, B. P. Flannery, S. A. Teukolsky, T. V. Vetterling, *Numerical Recipes in C*, Cambridge University Press, Cambridge, Massachusetts (1989).

[20] J. C. Moulder, E. Uzal and J. H. Rose, "Thickness and conductivity of metallic layers from eddy current measurements ", Rev. Sci. Instruments. Vol. 63, p. 3455 (1992).

[21] A. H. Kahn, "Impedance changes produced by a crack in a plane surface", Review of Progress in Quantitative NDE, edited by D. O. Thompson and D. E. Chimenti, Vol. 1, Plenum Press, New York, p. 369 (1982).

[22] V. G. Kogan,G. Bozzolo, and N. Nakagawa, "On boundary integral equation method for field distribution under cracked metal surface", Review of Progress in Quantitative NDE, edited by D. O. Thompson and D. E. Chimenti, Vol. 6A, Plenum Press, New York, p. 153 (1989).

[23] R. E. Beissner, "Boundary element model of eddy current flaw detection in three diemensions", Journal for Applied Physics, Vol. 60, p. 352 (1986).

[24] J. R. Bowler, "Eddy current field theory for a flawed conducting half-space", Review of Progress in Quantitative NDE, edited by D. O. Thompson and D. E. Chimenti, Vol. 5A, Plenum Press, New York, p. 149 (1986).

[25] B. A. Auld, G. McFetridge, M. Riaziat, and S. Jefferies, "Improved probe-flaw interaction modeling, inversion processing, and surface roughness clutter", Review of Progress in Quantitative NDE, edited by D. O. Thompson and D. E. Chimenti, Vol. 4A, Plenum Press, New York, p. 623 (1985).

[26] A. Sethuraman, James H. Rose, "Rapid inversion of eddy current data for concuctivity and thickness of metal coatings", Journal for Nondestructive Evaluation, Vol. 14, p. 39 (1995).